Review Article

Vivek Dhand, Yongseok Jeon[#], Jaehyeok Doh[#], Gyeonghun Han, Sanghoon Kim*, and Kyongyop Rhee*

Current status of synthesis and consolidation strategies for thermo-resistant nanoalloys and their general applications

https://doi.org/10.1515/ntrev-2022-0567 received March 28, 2022; accepted June 9, 2023

Abstract: Thermo-resistant nanoalloys are a new class of materials that combine high-temperature refractory compounds (such as carbides, nitrides, borides, and oxides) with nanoscale particles of metals, ceramics, or carbon. These composites exhibit remarkable thermal stability and antiablation/oxidation properties, making them highly attractive for various high-temperature applications in aerospace, energy, and high-temperature manufacturing. Despite their potential, the fabrication of these materials is challenging due to their complex synthesis and processing. Many researchers have summarized the challenges and suggested solutions to produce high-density, superior physicochemical properties of nano refractory materials for specific applications. Thus, in view of these perspectives, the present review provides an overview of the production criteria, processing,

These authors contributed equally to this work and should be considered first co-authors.

Yongseok Jeon: Department of Mechanical Engineering, Korea Maritime & Ocean University, 727 Taejong-ro, Yeongdo-gu, Busan 49112, Republic of Korea

Jaehyeok Doh: School of Mechanical and Material Convergence Engineering, Gyeongsang National University, Jinju-si, Gyeongsangnam-do, 52725, Republic of Korea

Gyeonghun Han: Department of Mechanical Engineering, College of Engineering, Kyung Hee University, Yongin, 446-701, Republic of Korea

and synthetic routes for producing high-temperature nano refractory material composites with exceptional thermal and anti-ablation/oxidation properties. The review also highlights the challenges encountered by researchers and their solutions for fabricating these materials. Potential applications of high temperature refractory materials are found in various industries, such as refractory ceramics, high-temperature components in wear resistant, neutron shielding, and high power-density microelectronics manufacturing to name a few.

Keywords: processing, synthesis routes, refractory, high temperature, anti-ablation, oxidation properties, applications

1 Introduction

Refractory materials are mainly non-metallic compounds or products comprising trace quantities of metals that have a thermometric cone close to 1,500°C as termed in ISO/R836 (which has been revised to ISO 836:2001). Further, the ISO 528:1983 determines the degree of refractoriness of the thermometric cone equivalents [1–3]. Generally, the sample refractory material cone is predominantly a triangular pyramid and is placed alongside the reference thermometric cone with a pre-determined softening temperature. It should be noted that there are few materials whose characteristics do not adhere strictly to this definition and are still considered conventional refractory materials. In the truest sense, the refractory materials are ceramic-based materials or products that can withstand high temperatures of ≥800°C. Several different compositions of refractory materials are used in different shapes, sizes, and forms for a wide range of industrial applications [1]. There are three main categories of refractory ceramic products including (i) refractory bricks, (ii) unshaped monoliths, and (iii) ceramic fiber-based products. Their applications include being used as the construction material for furnaces, thermal lining/insulation, heat recuperators (heat recycling in the regenerators), and as

^{*} Corresponding author: Sanghoon Kim, Department of Mechanical Design Engineering, Chonnam National University, 50 Daehak-ro, Yeosu, Jeonnam 59626, Republic of Korea, e-mail: shkim83@jnu.ac.kr, tel: +82-61-659-7382

^{*} Corresponding author: Kyongyop Rhee, Department of Mechanical Engineering, College of Engineering, Kyung Hee University, Yongin, 446-701, Republic of Korea, e-mail: rheeky@khu.ac.kr, tel: +82-31-201-2565

Vivek Dhand: Department of Mechanical Design Engineering, Chonnam National University, 50 Daehak-ro, Yeosu, Jeonnam 59626, Republic of Korea

structural or mechanical components for hot working aggregates, particularly in metal melt-processing, sliding gates, and filters. The internal layers of the furnace refractory lining (hot face), usually can resist temperatures in the range of 800−1,800°C and in certain instances temperatures up to ≥2,000°C. In addition to their high-temperature resistance, refractories are also resistant to the effects of sudden temperature gradients (thermal shock), mechanical, and corrosion, respectively [1].

Present day technological advances in materials research and processing requires high-temperature furnaces that have more stringent qualities, which, consequently, warrants the further development of advanced high-temperature heating elements [4,5]. At present the most used metallic heating elements are Mo [6-9], nano W [8,10–13], Ni–Cr–Fe [14–17], and Fe–Cr–Al alloys [18–22]. The disadvantage of these materials is that they are prone to oxidation at higher temperatures rendering them unusable after a few cycles of usage due to their limited temperature resistance range (Table 1). Recently, widespread interest in the development of non-metallic high-temperature-resistant heating elements including graphite [23-26], nano SiC [27-31], ZrO₂ [32-36], MoSi₂ [37-41], LaCrO₃ [42-47], and SnO₂ [48–50] has been reported. These heating materials exhibit anti-corrosive properties and are oxidation-resistant at high temperatures and contribute these qualities to the ceramic products in which they are included. Thus, various types of refractories are used in myriad industries and increase the shelf-life, and the resistance and refractoriness of the products [4,5].

Graphite is widely used because of its desirable electrical resistivity and conductivity, and its stability at higher operating conditions (>2,600°C) among the listed nonmetallic refractory based heating elements. However, the main disadvantage of graphite is that the graphite-containing elements require a vacuum or inert gas condition [4]. ZrO₂ heaters, on the other hand, can be utilized even in the presence of air at temperatures up to >2,200°C, but owing to its lower electrical conductivity below 1,000°C, additional resistive heating using a carrier gas or resistor element is required [4]. In contrast, LaCrO₃ offers a proven performance at elevated temperatures of 1,900°C in the presence of air, although the presence of any reducing gas, including water or hydrogen, at this temperature, reduces La, and compromises the structural state and phase stability of the heater. Additionally, the reduction of La contaminates the furnace material (charge) [4]. SnO2 is a widely used alternative for the more valuable RuO2-based micro-heaters specially designed for gas/chemical sensing instruments [4]. SiC is the most used ceramic heater but has a temperature limit below 1,500°C that is attributed to the crystallization of the amorphous phased SiO₂ at 1,600°C. Above 1,600°C the oxidation of SiC is markedly escalated. Additionally, the SiC-based heaters display a gradual increase in their electrical resistance during their lifetime, thereby, making them unsuitable for further use [4]. Other ceramic-based heating elements such as MoSi₂, display stable specific electrical resistance, higher corrosion resistance, electrical conductivity, and superior resistance against the high-temperature oxidation process [4,51]. Despite these advantages, MoSi₂-

Table 1: Different types and typical characteristic properties of metal based high melting point materials

Material	Melting point (°C)	Tolerable temperature limits (°C)	Specific application of the material	Prominent attributes and functioning considerations
Molybdenum (Mo)	2,622	1,600-2,000	Utilized in industrial	Very high price; mandatory to use it in
Tungsten (W)	3,390	2,300–2,500	furnaces operating at high	vacuum/protective/inert atmospheres
Niobium (Nb)	2,415	2,230	temperatures	
Tantalum (Ta)	2,996 ± 50	2,500		
Platinum (Pt)	1,770	1,400	High-temperature furnace with special prerequisites	Very high price; applicable under oxidizing environment
Iron–chromium–aluminum (Fe–Cr–Al) alloys	NA	(Cr ₁₃ Al ₄): 950 (Cr ₂₁ Al ₆ Nb): 1,350	Widely used in almost every furnace operating at	All the materials demonstrate good resistivity than other nickel-based
		(Cr ₁₃ Al ₆ Mo ₂): 1,250	high temperatures	alloys; affordable price; has lower
		(Cr ₂₅ Al ₅): 1,250		strength at high-temperature
		(Cr ₂₇ Al ₇ Mo ₂): 1,400		environments in comparison to other nickel-based systems; desirable oxidation resistance
Nickel-cadmium alloys	NA	(Cr ₂₀ Ni ₈₀): 1,200	Can be applied only in	Higher strength at high-temperatures;
-		(Cr ₁₅ Ni ₆₀): 1,150	furnaces operating below	facile process ability; slightly costlier;
		(Cr ₃ 0Ni ₇₀): 1,250	1,000°C	non-magnetic

based ceramic heaters do have some limitations including the easy and destructive oxidation at temperatures between 400 and 600°C which is also known as "pesting," an extremely low oxidation resistance above 1,700°C with lower mechanical and other structural properties, and a low creep resistance at higher temperatures. All these shortcomings in MoSi₂ ceramics can be improved by the process of intercalation using the borides of Mo, Ti, Zr, and Hf [52] or other materials, including SiC or Si₃N₄. Doping with SiC has imparted superior mechanical and oxidation resistance capabilities to MoSi₂ ceramics, but this also decreases the electrical conductivity of the MoSi₂ ceramic considerably, therefore restricting its usage as a heating element. There are other structural ceramics including ZrB2-SiC and HfB2-SiC, which are categorized as ultra-high-temperature ceramics (UHTC). These structural ceramics exhibit superior mechanical properties that exhibit a higher resistance towards thermal shock and oxidation [53,54]. Table 2 describes the characteristic features and the properties of several refractory-based UHTC materials [51-56].

Figure 1 illustrates the different types of refractory compounds that demonstrate very high melting points and Figure 2 illustrates the different physico-chemo-mechanical properties of transitional refractory compounds, respectively. Few authors have reported the optimized doping composition of ZrB2 with a 20 vol% of SiC [55]. This combination of compounds synergistically improves the mechanical and oxidation resistance property with a very small or negligible loss of electrical conductivity in the MoSi₂-doped ceramics. The tubular samples were fabricated using commercially available ZrB2, MoSi2, and SiC powders, which were examined at 1,894°C [55]. During the experiment, it was found that a surface oxide layer that developed was continuously endowed with several gas pores, induced by the vaporization of SiO₂ and boron trioxide B₂O₃. Additionally, the tubes did not crack on their surfaces despite being subjected to rapid heating and cooling rates of ~100 °C/min [4]. Regardless of its expense, HfB2 has various advantages when compared with its counterparts, e.g., ZrB2. In general, the kinetic oxidation resistance of HfB2 ceramic is 2-3 times greater than that of ZrB₂. This characteristic is attributed to the development of thermodynamically stable and stronger surface oxides [4]. The respective melting points of HfB2 and HfO₂ are approximately 130°C greater than those of ZrB₂ and ZrO₂, respectively, thus the eutectics melting temperature dependent on HfB2 and HfO2 concerning SiC, MoSi2, boron carbide (B₄C), C, and HfC is almost 100–200°C greater than the eutectics of ZrB₂ and ZrO₂, respectively. Furthermore, HfB2 has a higher ionization energy and greater chemical and structural stability in vacuum in comparison to ZrB₂ [4].

Figure 3 demonstrates the quality of nano SiC/B₄C composites produced by Taneja et al. [30].

Currently, there have been a few attempts to manufacture nano materials that have been introduced into modern power plants and high-velocity-based transport vehicles and these materials are capable of withstanding higher temperatures [57]. UHTC-based materials exhibit these properties and have displayed good operational performance even in oxidizing high-temperature environments with temperatures greater than 2,000°C [57,58]. Presently, composites of nano SiC, Si₃N₄, or SiC-coated carbon or their blended carbon composites and particular oxide ceramics are acknowledged as being effective high-temperature-resistant construction materials. The carbon-carbon composites are mechanically strong materials even at higher temperatures; however, the main drawback is the process of destructive oxidation which follows above 500°C. The oxidation makes them brittle and there is a loss of functionality [57,59]. In contrast, composites of nano SiC/Si₃N₄ are highly resistant against oxidative stress even above 1,550°C, but the drawbacks associated with these composites is the low resistance to thermal shock, vapor induced severe corrosion at higher temperatures, and the accelerated decline in the oxidation resistance due to the presence of the metallic cations arising from the salts of alkaline earth and alkali materials, respectively. These limitations substantially impede their specific application [60] and the decreased electrical conductivity of the nano SiC/Si₃N₄ based composites prevents their electroerosion (electrical discharge machining) process for making complex-shaped components [57].

Most of the borides of the d-block elements (transitional metals; TMs) are promising materials that offer a good foundation for the development of modern nano UHTCs, because of the metallic interaction and bonding within the TM layers and higher thermal (ZrB₂ ~ 130 W/m K) and electrical ($ZrB_2 = 10^7 S/m$) conductivities arising due to the strong covalent bonding within the B-layers. The compounds exhibit high elastic modulus and hardness, and a comparatively lower coefficient of thermal expansion (CTE; $6-7 \times 10^{-6} \, {}_{\circ}\mathrm{C}^{-1}$). Due to the combinations of the thermo-physical properties and their synergistic effects, borides, including ZrB₂, effectively demonstrate higher thermal shock resistance [61]. Figure 3 depicts a nano SiC/B4C composite prepared by Taneja et al. [30].

On the other hand, the oxidation resistance of refractory di-boride is evaluated by the development of a protective glassy surface layer of nano sized B₂O₃ which prevents the diffusion of oxygen into the refractory material [57,58,61]. Nonetheless, the B₂O₃ starts to vaporize quickly when the temperature reaches above 1,100°C thereby, decomposing

Table 2: Basic physical, mechanical, and oxidation properties possessed by the various UHTC

Material	Material Crystal structure		Melting Density point (°C) (g/cc)	CTE (α; 10 ⁻⁶ K ⁻¹)	Thermal conductivity (W m ⁻¹ K ⁻¹)	Electrical resistivity (μΩ cm)	Elastic modulus (GPa)	Hardness (GPa)	Fracture toughness (MPam ^{1/2})	Flexural strength (MPa)	Oxidation resistance (°C)
Borides TiB ₂	HCP	3,225	4.5	8.6	60–120	9–15	200-560	25–35	4-5	700–1,000 (3-	<1,200
ZrB ₂	HCP	3,200	6.1	6.8	60	10–32	340–500	20–25	4 v	point) 300-400 350 450 44	1,200–1,400
TaB,	ב ב	3.040	7.11. £	c. 8	50 N	- 33	748-551	21-28	AN 4		1,200-1,400
NbB ₂	HCP	3,036	6.9	NA NA	¥ Z	NA	637	21	4	414 (3-point)	NA YES
Carbides HfC		3,900	12.8	9.9	20	109	300–340	26	NA	250–350	<800; >1,800
TaC	FCC	3,800	14.5	6.3	NA	30	470-540	14–19	3.4	002-009	<1,400
ZrC NbC	U L	3,530	6.6	6.7	20.5 NA	63 74	480	27	2 NA	400 (3-point) NA	<800; >1,800 <800: >1,800
TiC		3,100	4.9	7.7	NA		451	NA NA	NA	NA	NA
Nitrides											
NIT	FCC	2,950	5.4	9.3	19.2	NA	NA	NA	NA	NA	NA
ZrN	FCC	2,950	7.3	7.2	20.5	NA	380	NA	NA	330	<800
НfN	FCC	3,385	13.9	6.9	23	NA	420	NA	NA	290-350	<800

Note: HCP: hexagonal close-packed; FCC: face centered cubic [51–56]. Tabular data adapted, reprinted with permission from Golla et al. [61].

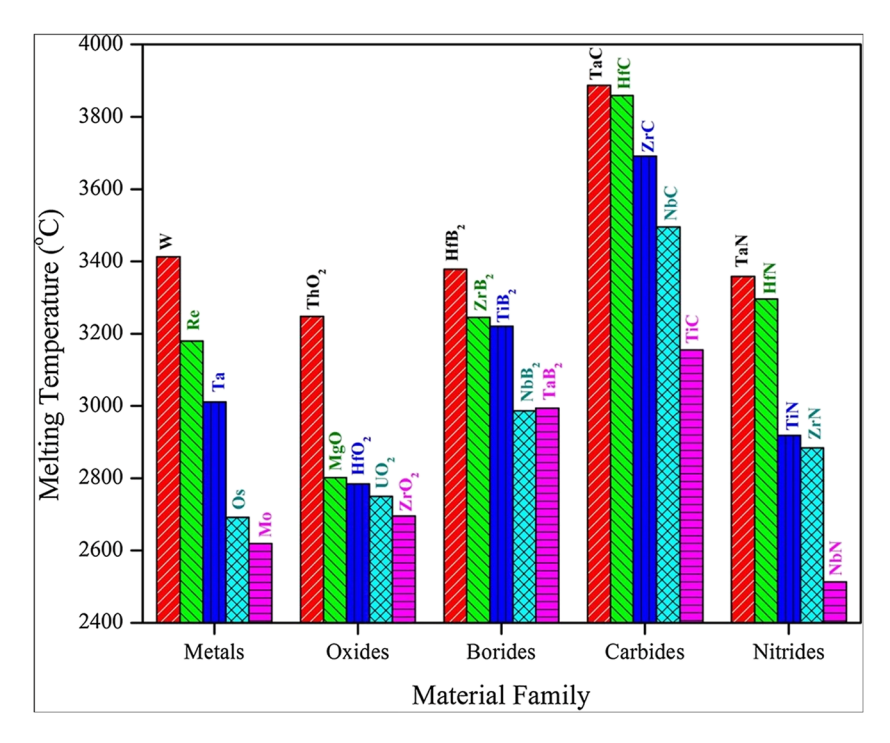


Figure 1: Melting points of different refractory materials based on their compound type (Fahrenholtz *et al.* [56]). Reprinted with permission from The American Ceramic Society, A John Wiley & Sons.

the protective barrier. The decomposition of the barrier can be halted and avoided by introducing dopants into the lattice of the di-boride as stated previously. The common siliconbased doping agents are SiC, TaSi2, ZrSi2, and MoSi2 in the refractory domains [57,58]. When the temperature reaches 1,600°C, the formation of glassy borosilicate (SiO₂) takes place within the doped refractories, and this layer thus offers good stability and protective attributes to the di-boride refractories. An alternative option to improve the high-temperature oxidation resistance in ZrB2 is to synthesize an alloy by introducing TaB₂, which would produce a bimetallic boride (Zr,Ta)B₂ ceramic solid solution [57]. Opila et al. reported that their ZrB2-SiC composite exhibited an excellent oxidation resistance against air when the temperatures reached 1,627°C [62]. The resistance was considerably enhanced by the addition of a silicate (TaSi₂) and a di-boride (TaB₂) to the ZrB₂-SiC composite, which inhibited the ZrO₂ phase transition from the tetragonal and monoclinic systems, respectively. The inhibition of the transition in the complete preservation of the morphological integrity of the oxide glassy film reduces the rate of oxygen transfer into the refractory material [57]. Figure 4 depicts the refractory SiC, ZrO₂, oxide-fiber/Mo-based alloy matrix composites fabricated using different routes.

In recent times, there has been a growing interest in the synthesis and consolidation strategies for thermo-resistant nanoalloys. These materials exhibit high thermal stability and mechanical strength at elevated temperatures, making them attractive for potential applications in various fields such as aerospace, energy, and automotive industries. Researchers are continually exploring new synthesis and consolidation strategies to improve the properties of these materials and enhance their performance in different applications. The extensive attention this topic has received underscores its significance and relevance in current research, and further advancements in this area will undoubtedly have a substantial impact on various industries [4,5,60,61]. Additionally, authors believe that synthesizing thermo-resistant nanoalloys through consolidation strategies presents several obstacles, including attaining high density, regulating grain size, and achieving uniform distribution of components. Maintaining composition and preventing contamination are additional challenges. The selection of consolidation technique is also crucial in determining the material's final characteristics. Moreover, upscaling production while preserving desired features and minimizing expenses remains a substantial challenge in the field of thermo-resistant nanoalloys.

From their discovery to the present, several types of refractory elements, compounds, and alloys have been developed which have higher melting points nearing 1,670°C (3,006°F) or greater. These include elements such as W, Ta, Mo, Ti, Hf, Zr, Nb, Cr, V, Re, *etc.*, and the alloy systems of W, Nb, Mo, Ti, Cr, Cr/Zr mixed alloys, Rh, and Ta based alloys to name a few. Several of these refractory materials are developed in the

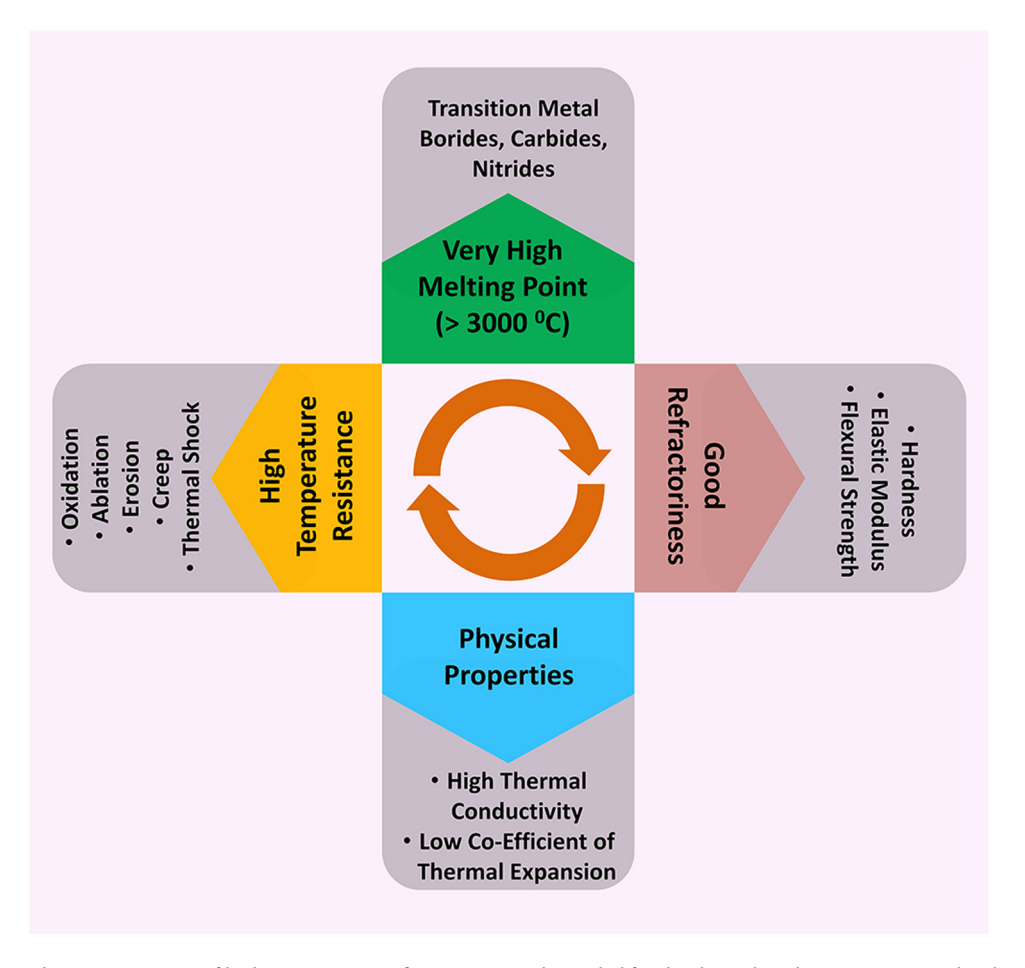


Figure 2: Different characteristic traits of high-temperature refractory materials needed for the desired applications. Reprinted with permission from Elsevier, Golla *et al.* [61].

form of strips, sheets, foils, bars/pipes, threads, and metallurgical powder-based products. Thus, this comprehensive review describes in detail the present-day synthesis routes used for various refractory nano materials and their applications in various sectors taking into account the history, types, and the thermal properties of the refractory materials. The review covers a time period ranging from 2003 to 2022, with a greater focus on the most recent 5 years, specifically from 2018 to 2022.

2 Processing/synthesis routes

Several processing/synthesis routes are available for the synthesis of refractory nano materials. These are sol–gel [63], co-precipitation [64], hydrothermal [65], mechano-chemical [66], and molten-salt processes [35,67], combustion synthesis [68], spark plasma sintering (SPS) [69], microwave synthesis [70], ultrasonic-spray pyrolysis [71], solid-state reaction or the ceramic [72], and hot press methods [73–76].

Nevertheless, due to the high expenditure and the highly advanced technical process, these novel technologies are only at the bench-scale laboratory stage. All the materials listed in Section 1 behave as refractory nano materials which exhibit high temperature-resistant behavior which also categorizes them as UHTCs. However, the manufacturing process, extremely high-temperature processing, shape limiting, and densification procedures remain challenging. Generally, few processes such as pressureless sintering (PS), reaction sintering (RS), SPS, HP/hot-isostatic pressing (HIP), and plasma/ vapor deposition are often employed to achieve the desired outcome [77]. In principle, every manufacturing route has its pros and cons, the key to any favorable outcome for the UHTCs depends purely on the process to manufacture a dense material exhibiting good crystallinity and having superior microstructures. Globally, there is a huge demand for the UHTCs, and research is ongoing to develop novel, facile synthesis technologies that can produce superior quality, highly economical, and easily affordable components, and materials. Many technologies are important in the manufacture of the

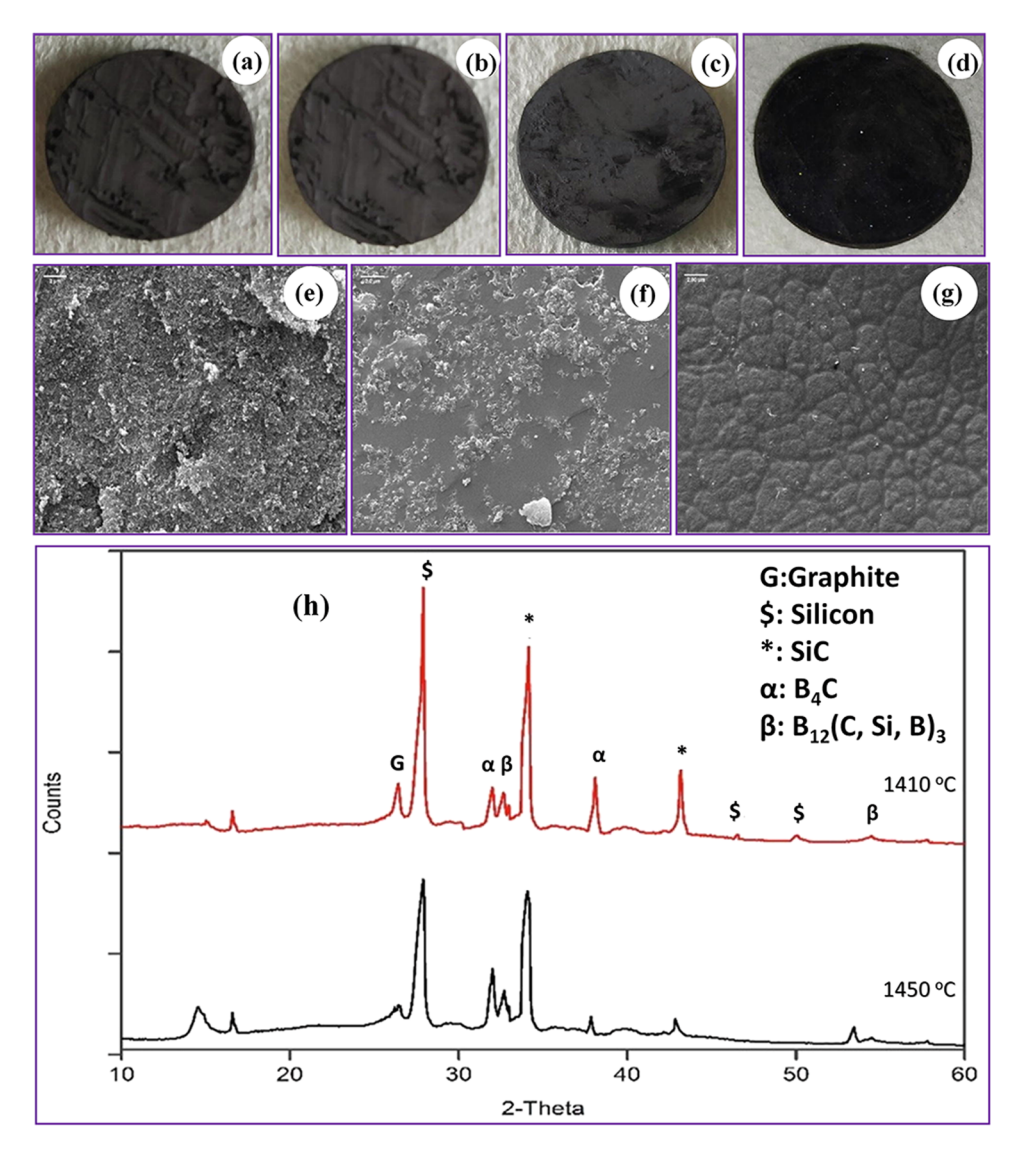


Figure 3: SiC/B₄C composite pellets (uniaxially pressed) obtained from powdered boron carbide/graphite/silicon. (a) Pre-fired pellet; (b) pellet after heating to 1,350°C; (c) pellet after heating to 1,410°C; (d) pellet after heating to 1,450°C; SEM images of the powdered pellets fired at the following temperatures: (e) 1,350°C; (f) 1,410°C; (g) 1,450°C; (h) X-ray diffractograms of the sintered samples. Reprinted with permission from Elsevier, Taneja *et al.* [30].

refractory materials, and this section will cover in detail the research thus far performed in the synthesis of refractory materials having various compositions using other synthesis routes.

2.1 PS process

This process involves the use of extended periods of sintering the compact powders at very high temperatures (1,500–2,000°C) based on the chemistry of the powder in the absence of any applied pressure. Additives that ensure the densification (Figure 5) and uniform grain structure of the compacts either before the onset of the liquid phase

or solid state during the sintering process are also added under a controlled atmosphere (Figure 6). By judiciously selecting the components and raw materials the process aids in achieving the desired densities which are very close to the theoretical estimates [78,79]. Advantages of PS includes lower cost, offers better control over composition, reduced shrinkage of the samples with more retainment of its original dimensions, and improved density and strength of the final product. Whereas, the disadvantages of the process are longer processing time as it relies solely on heat to achieve the desired density, limited to certain materials such as ceramics, and may not work well with more complex materials, the process is more susceptible to defects such as cracks and voids due to heat employed to

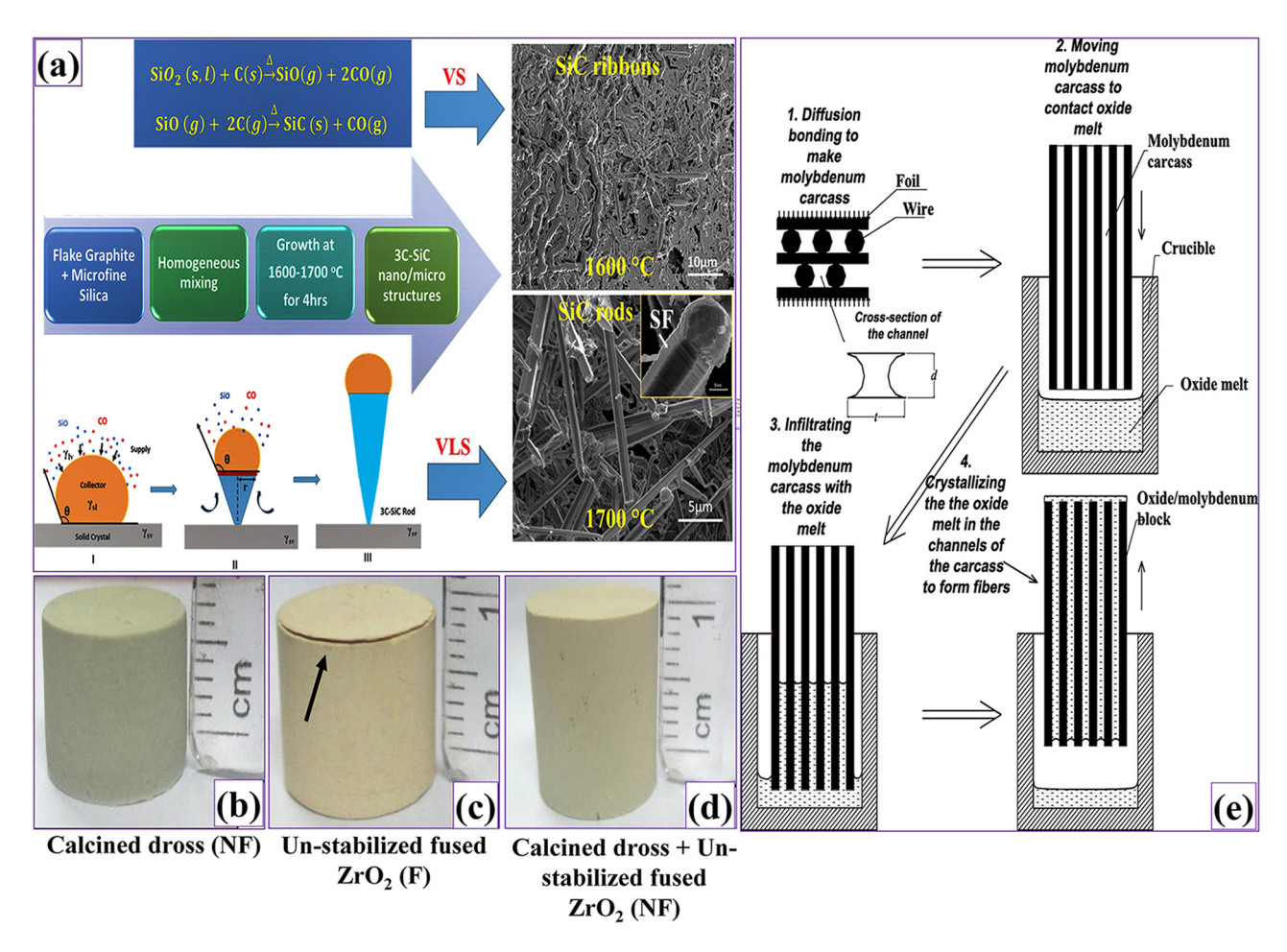


Figure 4: (a) Refractory SiC produced at high temperatures of 1,600–1,700°C in the furnace along with the possible growth mechanism as observed during the carbothermal reduction reaction. Reprinted with permission from Elsevier, publishers of ref. [31]. (b–d) Images shows different industrial grade zirconia dross structures sintered and tested at 1,150°C for thermal shock cycling (NF = not failed; F = failed; Ramaswamy *et al.* [32]). Reprinted with permission from Elsevier. (e) Four stages in the synthesis of oxide-fiber/molybdenum-based alloy matrix composites at 1,250°C during second stage and followed by heat treatment at 2,000°C during third and fourth stage by the internal crystallization method devised by Mileiko *et al.* [41]. Reprinted with permission from Elsevier.

achieve densification and it is limited to certain shapes and sizes [80].

Luo *et al.* studied the effects of different loadings of MgO–LiF as a sintering additive on the thermo-mechanical properties of pressureless sintered $\mathrm{Si_3N_4}$ ceramics obtained at 1,620°C. The ceramics had a relative density of 92% when 7 wt% MgO and 3 wt% LiF were used as additives. The thermo-mechanical properties exhibited by the ceramic included a high bending strength of 556.73 (±10.18) MPa, hardness of 9.07 (±0.07) GPa, fracture toughness of 6.02 (±0.29) MPa/m^{1/2}, and thermal conductivity of 47.59 (±0.03) W/(m K). The improvement in the thermo-mechanical properties is attributed to the phase transition from the α to β phase due to the addition of LiF to $\mathrm{Si_3N_4}$ ceramics. The dissolution and re-precipitation of the liquid phase α - $\mathrm{Si_3N_4}$ is initiated along the Ostwald ripening process due to reaching

the saturation point in the dissolved state. In any given scenario, the viscosity of the liquid phase is crucial in the materials phase transition. The lower the viscosity, the more the mass transfer contributes to the phase transition of the material. The formation of a silica phase in the compact due to supportive sintering additives also helps to decrease the viscosity of the material [81].

Allemand *et al.* compared two processes to sinter hexagonal barium aluminosilicate (BAS) monoliths using SPS and a novel ultra-fast pressureless sintering (UFPS) technology. The monolith was sintered between 1,590°C and 1,760°C, which is the thermal stability range of the material. The researchers found that the SPS process could only fabricate small portions of the BAS monoliths due to the manifestation of a thermal gradient that resulted in the partial melting of the monoliths. However, UFPS was able

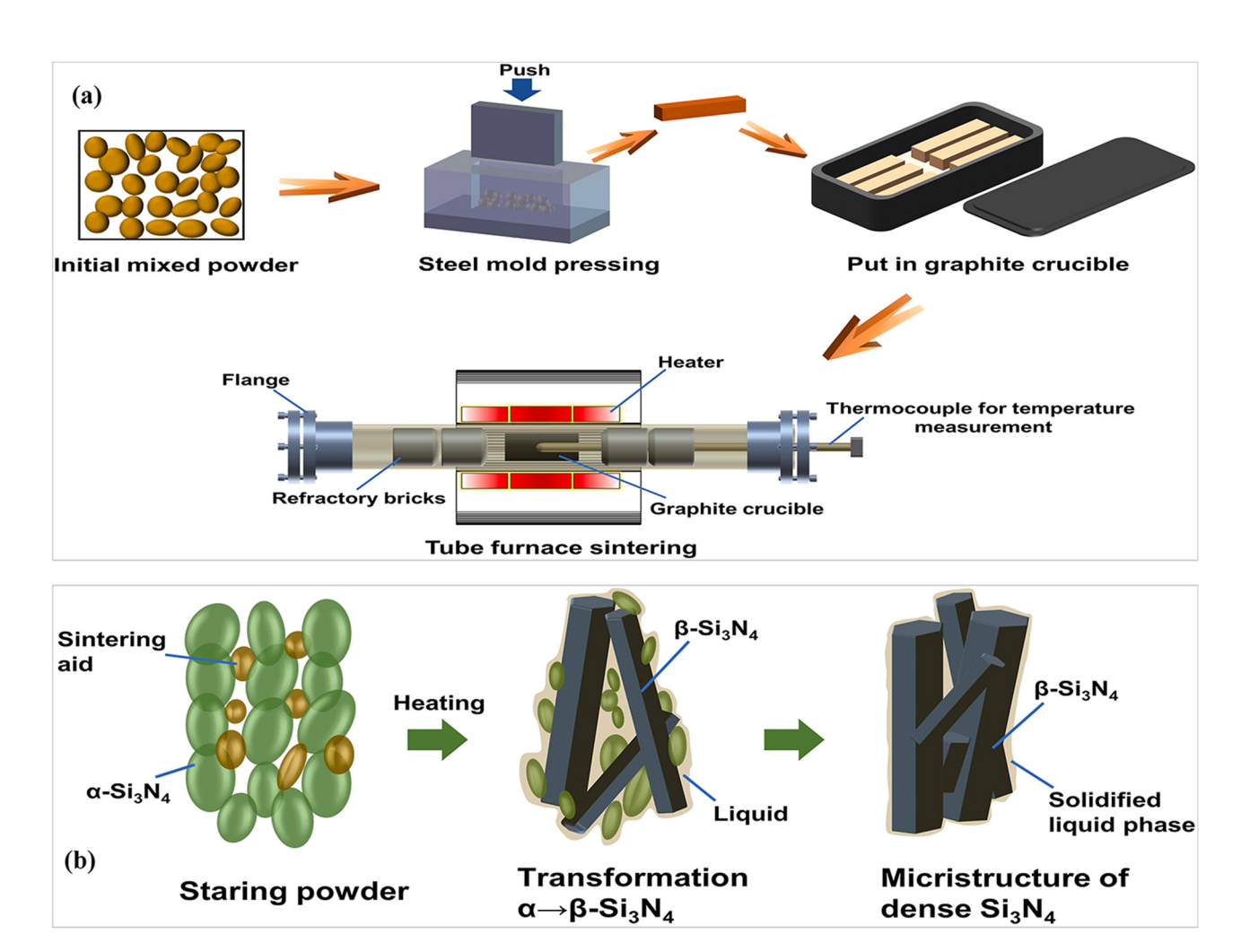


Figure 5: (a) Schematic of silicon nitride ceramic preparation and (b) densification process of silicon nitride from $\alpha \rightarrow \beta$ phase transition. Obtained with permission from ref. [81].

to process and fabricate the complex and larger shapes of the monoliths with equal efficiency and offers improved temperature control during the sintering process concerning SPS. A 1:2:2 molar mixture of powders including BaCO₃, Al(OH)₃, and SiO₂ quartz was used to synthesize BAS monoliths, respectively. All the powders were mixed and homogenized ultrasonically in pure ethanol at pH = 11 for 4 min and later dried for 2 h at 120°C. A portion of the powdered mixture was sintered by the SPS process, where it was kept in a graphite pressing (mold) device with two pistons and a single matrix. Initially, a BN3 layer was coated onto the carbon sheet (Papyex®) within the mold, and this coating aided in protecting the powdered oxide samples. The SPS functions under the temperature control (optical pyrometer) centered on a small orifice on the graphite mold surface. The graphite mold was encapsulated with a graphite mat (felt) to mitigate the thermal gradient and any heat loss that may have occurred inside the

sample. The other portion of the powdered sample was sintered using the UFPS process, which is very similar to SPS, but excludes any electrical current passing through the graphite die or sample. The obtained green body was thereafter fabricated from the powders using compaction at 100 MPa within the mold. Allemand et al. employed three step based thermal cycles for their samples using both SPS and UFPS. Initially, the researchers maintained a heating ramp rate of 100°C/min to reach a final temperature of 900°C, which was maintained for 1 min; the dehydration process starts at 900°C by converting Al(OH)₃ into alumina (Al₂O₃). Second, the increase in temperature from 900 to 1,150°C at a heating ramp rate of 80°C/min and a holding time of 10 min enables the formation of intermediate species such as barium aluminate/silicate. Third, the final step involves increasing the temperature to 1,600°C at a ramp rate of 100°C/min and a holding time of 10 min; it is at this stage that the BAS forms. UFPS does not involve any pressure

Pressureless Sintering (a, b); Reactive Pressureless Sintering (c-g)

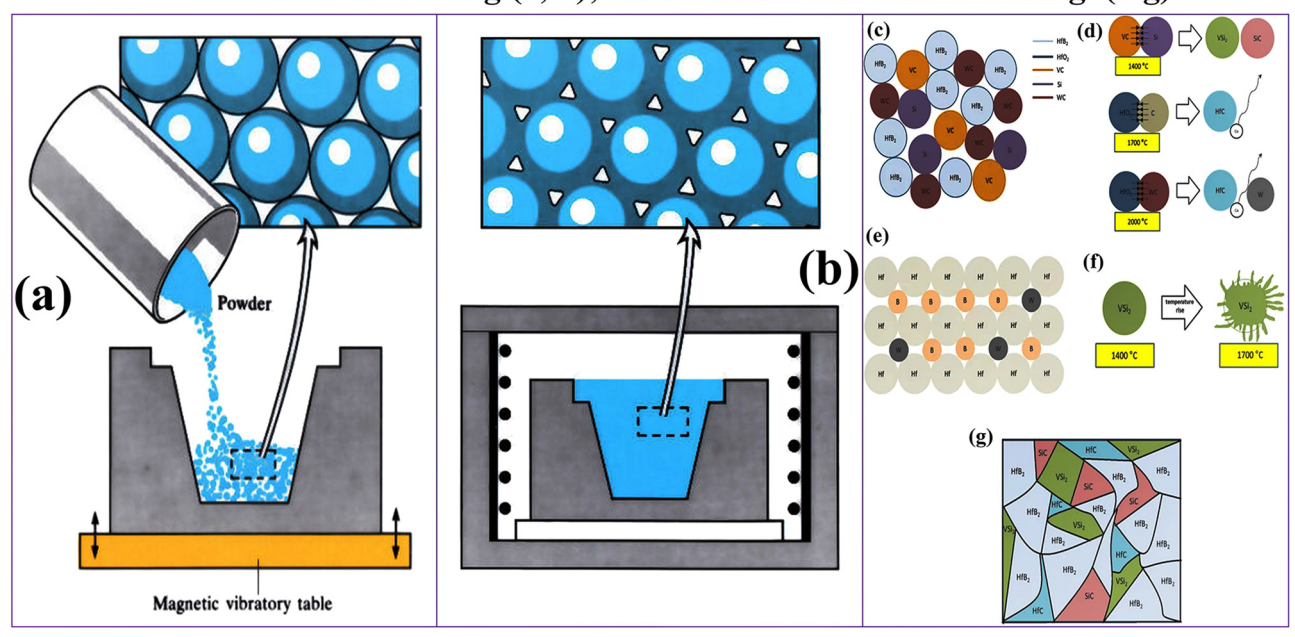


Figure 6: Depicts the PS and reactive PS processes. (a) Step 1: Where a loose bound mixed powder of the refractory precursors is filled into the metal die which is vibrated magnetically to settle up; (b) step 2: the powder and die are sintered in a sintering furnace at a desired temperature to get the final products; the image shows reactions as observed during the reactive PS process of HfB₂–SiC–VSi₂ composite. (c) post 5 h milling shows dispersed particle arrangement; (d) reaction at densification phase; (e) formation of a solid solution of (Hf,W)-B due to tungsten (W) getting inter-substituted in HfB₂ structure; (f) the melting of VSi₂ at 1,700°C; and (g) the obtained composite (HfB₂–SiC–VSi₂) with its final microstructure, post its sintering at 2,150°C. The images (a and b) are reprinted with permission from OpenLearn content, Copyright holder: The Open University© [78]. Images (c–g) are reprinted with permission from Ghadami *et al.* [79], Springer Nature.

sintering procedure. Whereas, SPS involves the use of a high pressure of 40 MPa under vacuum conditions in all situations and for all the steps [82]. Refining the grain microstructure of the as-sintered material from an ultra to nanocrystalline size with decreased porosity and uniform homogeneity is highly desired. The nanocrystalline size enhances the reliability of the material and improves the properties of the material, including malleability. There are some processes, such as doping or field assisted sintering that inculcate increased thermo-mechanical properties with good purity and shape molding options for specific applications such as 3D printing and sputtering targets. It is challenging to yield pure phased elemental refractories using the solid-state PS that is usually performed at temperatures higher than 1,500°C. The higher temperature induces a capillary driving force during the sintering process that results in a synchronal grain growth in size and coarseness. This is a major problem, especially when producing nano-powdered refractories. PS, in general, involves a two-step sintering process: initially, the green body is compacted and heated to a certain high temperature (T_1) without the final temperature being maintained for any period. This causes the relative density ρ to be approximately greater than 70-80%, and the shrinkage of the

relative pore size, ensuring that the channels alongside the grain size are at a high thermodynamically unstable mark. Later, the green body is cooled to a lower temperature T_2 (e.g., 100–200°C lower than T_1) and is maintained at this temperature for a period so that the full density is achieved. The second step allows sintering at T_2 that helps in densifying and inhibiting the grain growth. A completely suspended grain size can only be achieved using best practices. This process has yielded a beneficial Lifshitz-Slyozov-Wagner-Hillert grain size uniformity with a homogenized micro to nano-structure and has successfully constrained the grain size of yttria to ~30 nm; additionally, the yttria has enhanced properties [83]. Dehghani et al. have recently reviewed the effects on the properties of introducing AlN-Y₂O₃ into pressureless sintered SiC ceramics [84]. Nguyen et al. explored the anatomical and morphological structure of porous ZrB₂-SiC-AlN composites that were fabricated using PS at 1,900°C, using electron microscopy [85]. Li et al. synthesized dense ultrafine-grained W using a two-step pressureless sintered process and achieved a 99.6% theoretical density at 1,600°C when their samples were sintered for 3 h. The researchers also observed no changes in texture, second-phase impurities, no abnormal grain growth, or grain boundary (GB) liquids

even after cooling the samples [86]. Jafari et al. studied the effects and behavior properties of ZrB₂–SiC nanocomposites by introducing HfB2 into the microstructures produced via PS for 1 h at 2,100 and 2,150°C using MoSi₂ and B₄C as sintering catalysts, respectively. With the increasing HfB2 content, there was an apparent reduction in porosities. Moreover, the presence of MoSi₂ engendered a partial molten phase during the sintering process that markedly improved HfB2 diffusion into ZrB₂. The apparent change and reduction in the porosity and density occurred in the B₄C catalyzed samples. When the samples were compared with micron-sized SiC and SiC_n (nano) the researchers found that the SiC_n were much smaller and finer than the SiC [87]. Similarly various high-temperature materials such as silicon nitride-barium aluminosilicate (Si₃N₄/BAS) [88], nano (Ca,Sr,Ba)ZrO₃ [89], nano Ti₃SiC₂ interlayer phased SiC [90], Gd₂O₃/Yb₂O₃ infused O'- SiAlON/Si₃N₄ [91], Al₂O₃-mullite-ZrO₂-SiC [92], calcium magnesium aluminosilicate/Yb₂SiO₅-YSZ [93], nitride-based calcium hexaaluminate $(CaAl_{12}O_{(19-1.5x)}N_x)$ [94], nano $TiB_2-CrB_2-WB_2$ [95], ZrB_2 ceramics co-doped with graphite and TiC [96], liquid phase sintered B₄C infused SiC-Al₂O₃-Y₂O₃ composite systems [97], B_4C -Co and ZrC-Co cermets [98], Zr B_2 -MoSi₂ [99], MgF₂ + Y₂O₃ + MgO/β-silicon aluminum oxynitride (SiAlON) ceramics [100], (Ni, Co, WC)/TiB₂ [101], α - β -YbF₃-Si₃N₄ [102], ZrB₂-TiB [103], ZrB₂-SiC-TiB₂-B₄C [104], Ta_{0.8}Hf_{0.2}C/MoSi₂ [105], α-SiC/ (Al₂O₃, Lu₂O₃, Er₂O₃, and CeO₂) [106], AlTiB/diopside:(MgCa (SiO₃)₂ [107], Al₂O₃/barium-magnesium aluminosilicate [108], B₄C-TiB₂/TiO₂ [109], TiB₂-40 wt% TiN [110], Ni_xAl_yTiC [111], Zn/ Ce_{0.8}Gd_{0.2}O_{1.9} [112], and HfB₂-SiC-VSi₂ [79] have been produced and processed by PS. This list is not comprehensive.

2.2 RS

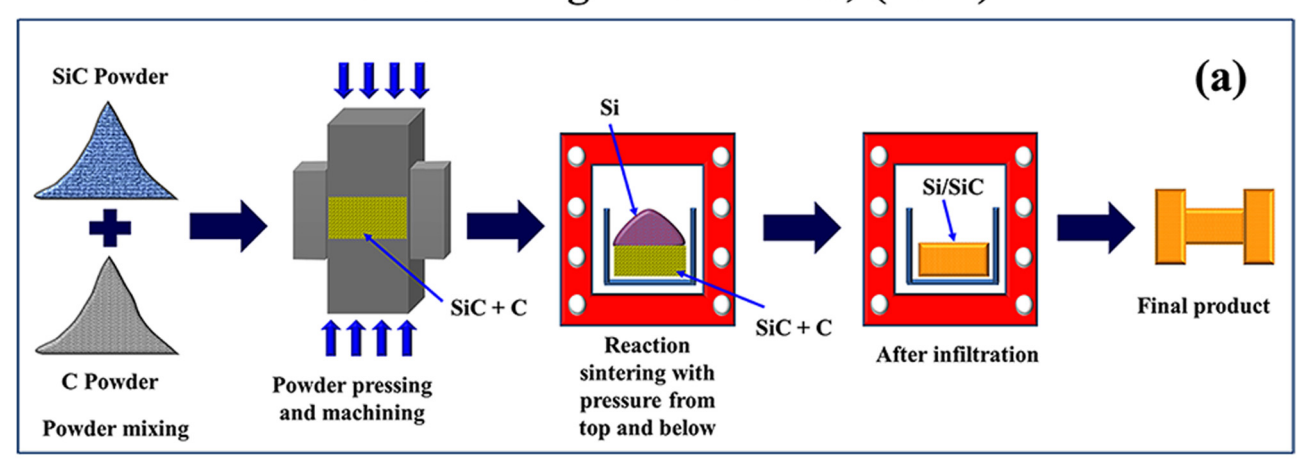
This process relies on the in situ synthesis of UHTC via a chemical-based reaction, where a hard, compact powder sample is converted into a UHTC material either by a solidstate reaction process or by vapor-phase deposition. In this way, the material obtained has a constrained density gradient. One of the benefits of RS is that it can lead to materials with enhanced mechanical properties like strength, hardness, and wear resistance, due to the high material density achieved. Additionally, the technique allows for the production of high purity materials with minimal impurities, as the reaction can take place in a controlled environment. However, RS also has its drawbacks, which must be considered. This process can produce complex shapes and intricate parts, as the starting materials can be shaped before the reaction occurs. Furthermore, this method of manufacturing is cost-effective, and results in high-quality materials with minimal waste [113]. Despite its advantages, RS also comes with certain drawbacks. The process necessitates high temperatures, which can be energy-intensive and may even cause material degradation. Additionally, it involves a long processing time and may have limited material options available for forming the desired product. Finally, there is limited control over the reaction, which can lead to the production of unwanted byproducts or incomplete reactions. Figure 7 depicts a general process occurring during the RS process.

Tsuno et al. developed a novel, highly robust nano SiC using the RS method. The nano SiC was a lightweight, attractive optical mirror with more than twice the bending strength in comparison to other SiC materials. The SiC produced by the RS method is polished by a diamond slurry that is devoid of pores and is extremely compatible with the visible and infrared region even excluding the chemical vapor deposition (CVD) based expensive SiC coating. The material exhibited a mean bending strength of 854 MPa, Young's modulus of 400 GPa, fracture toughness of 3.3 MPa m^{1/2}, CTE of 3.9×10^{-6} /K (RT-799.85°C), specific heat capacity of 680 J/kg/K, and thermal conductivity of 130 (W/m/K). They state that the material is well suited for use in the manufacture of large-scale objects due to the novel fabrication process that ensures very little shrinkage and involves a lower temperature. The material was synthesized by mixing SiC and C and was spray dried; it was later cold pressed to form a green body. The green body was thereafter reaction sintered at 1426.85°C (1,700 K) under extreme vacuum conditions during which the molten Si reacted with the C in the green body to yield the desired SiC. Some traces of Si remained. The product was then mechanically finished to the desired shape and used in optical applications for astronomy [114]. Xiaoju et al. synthesized a SiC/B₄C composite using Si infiltration in the RS method which exhibited excellent mechanical attributes. The dynamic strength results of the SiC/B₄C composite shows a peak value of 1,000/s and its strain continuously increased with the increase in the strain rate. The authors observed three deformation regions in the composite which, including inelastic deformation, failure rapid loading regions during the analysis for dynamic loading [115]. Luo et al. synthesized single phased Ba₂Ti₉O₂₀ (BTO) using the RS method with TiO₂ and BaCO₃ as precursor materials after sintering for 10 h at 1,150°C. The overall reaction activation energy calculated was approximately 386.17 kJ/mol. The researchers observed that the formation sequence of the phases related to the RS process followed the sequence described in Eq. (1).

$$BaTi_4O_9 \rightarrow BaTi_4O_9 + BaTi_5O_{11} \rightarrow Ba_2Ti_9O_{20}.$$
 (1)

The composite had pores on the BTO grains because of the sintering which may be due to the absence of oxygen

Reaction sintering: Tsuno et al., (2004)



Chemical reaction during Reaction sintering

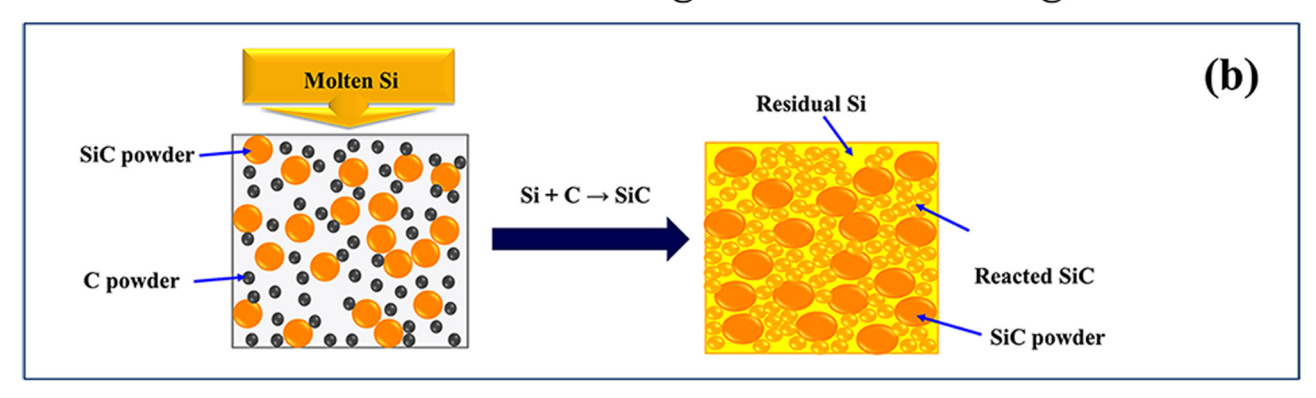


Figure 7: Refractory SiC produced at high temperatures of 1426.85 °C (1700K) by reaction sintering. Reprinted with permission for ref Tsuno *et al.* (2004) [114] from SPIE Journal Publishers under a Creative Commons Attribution 4.0 Unported License (CC BY).

vacancies and elements. However, the surface of the ceramic surface was very rough, and the texture is attributed to the heterogeneous distribution of Ba on the exterior surface of the BTO grain which contributes to the Ti enrichment. In a typical process, the pure powders of TiO2 and BaCO3 were ball milled in distilled water using ZrO₂ grinding balls for 6 h to form a slurry which was dried at 60°C. The dried slurry was sieved and mixed with a binder solution of polypropylene glycol. The mixture was not calcined, but it was pulverized, mixed, and dried. The obtained uniform dried powders were subsequently compacted at 200 MPa to form a green body which was thereafter debinded for 2h at 600°C and later sintered for different soaking times in the temperature range of 900-1,150°C. The optimized microwave dielectric property of the BTO that was treated for 10 h at 1,150°C was $\varepsilon_{\rm r}$ = 34.5, with a $Q \times f$ of 11,400 (at 5.7 GHz) and τ_f of 2.89 ppm [116]. Likewise, several researchers have synthesized other combinations of high-temperature materials using the RS method for example: Zr_{1-x}Sn_xO₂ reinforced alumina-mullite refractory

[48], nano-powdered $BaZr_{0.8}Y_{0.2}O_{3-\delta}$ [117], (Ti,Zr) B_2 –(Zr,Ti)C [118], mullite- Al_2 Ti O_5 [119], W-ZrC [120], and nano sized MgO–CaZr O_3 – β -Ca $_2$ Si O_4 [121].

2.3 SPS

This process involves the flow of an alternative electric current, through the material while the material is being hot pressed. This process is relatively new in the present era, and it allows for the faster sintering of a material. However, this process along with hot pressing (HP) can produce only a defined cast of simple shapes, which would necessarily involve the use of another costly machining process for the manufacture of intricate engineering components. SPS, similar to PS and RS techniques, has several advantages such as the ability to create high-density materials, shorter processing time, cost savings, and uniform heating throughout the sample. Furthermore, SPS allows

for the development of more uniform microstructures, improved properties, and greater control over grain size. It is applicable to various materials, including metals, ceramics, and composites. However, the SPS method has a few drawbacks, such as high equipment costs, limited sample size, scalability challenges, and process control difficulties [80,122]. Paul et al. (2021) synthesized ZrB2-MoSi2 composites and studied the effect of adding silicon carbide whiskers (SiC_w) to the composite to understand the wear performance. The composite ZrB2-MoSi2-SiCw (ZMSw) was produced using the SPS method during which the powders of pure raw ZrB₂, MoSi₂, and SiC_w were mixed in acetone at different stoichiometric ratios in a planetary mono-ball mill using WC grinding balls for 6 h at ~250 rpm. The milled powders were heated for 1h at 300°C to remove the acetone and were later dried and ground to a fine consistency and packed in a graphite foil lined graphite die for sintering using the SP process with multi-step sintering in the range of 1,400-1,700°C under a vacuum. A uniaxial pressure of 60 MPa was applied throughout the sintering

cycle. The SPS heating rate was 100° C/min. The tribological results indicated that the self-lubricating tribo-oxide layer that formed during the frictional heating significantly improved the composite resistance. The operational wear maps show that the tolerant workable load limit for the ZMS_w lies between 20–40 N [123]. Figure 8 depicts the general process occurring during the SPS process and the differences between the conventional sintering and SPS process following the different process stages and the passage of the current in the nano powders during the reaction [124].

Chakravarty *et al.* (2021) fabricated highly dense, super strength nano W–TaC–Ta $_2$ O $_5$ (similar to the W-MC system, where M = Ta, Zr, Hf, Ti) by the SPS method. The fabrication was performed under high vacuum conditions (3 × 10^{-4} mbar) and in the temperature range of 1,773–2,273 K (1,500–2,000°C) under an applied stress of 25–100 MPa. The synthesis involved mixing the raw powders of W and TaC under an Ar atmosphere in a high energy ball mill using WC balls for 2 h at a speed of 250 rpm. Later, the milled

Spark Plasma Sintering Process

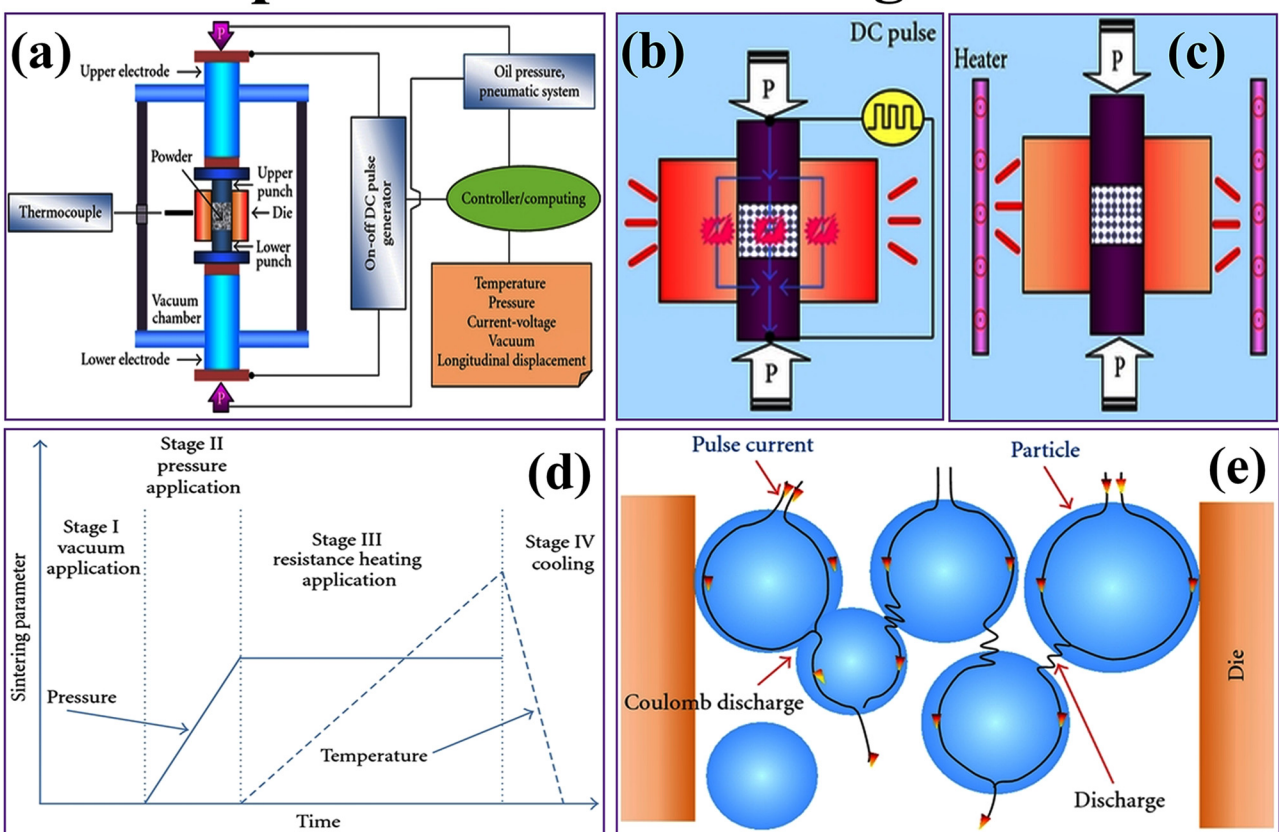


Figure 8: (a) A generalized spark plasma process scheme; comparability between (b) SPS and (c) conventional sintering methods; (d) graph depicting different stages of a typical SPS process; and (e) the passage of direct current (DC) pulse through the powdered particles during an SPS reaction. Reprinted with permission from ref. [124] from Hindawi.

mixture was reduced in H₂ for 2 h at 1,500°C and thereafter subjected to the SPS process [125]. Azevêdo et al. used the SPS method to synthesize nano phased (300-200 nm sized) Al₂O₃-WC-Co composites for abrasive machining application. The raw materials (Al₂O₃, WC, and Co powders) were initially mixed in a high energy mill. Subsequently, they were wet milled in the presence of ethanol, using carbide balls for 50 h at 450 rpm. The slurry was thereafter spread to dry on Al foil to remove ethanol. After the mixture was dried, it was placed in a graphite die and SPS was performed at 1,550°C at a heating ramp rate of 65°C/min under 40 MPa of pressure and 100 Pa of vacuum, with a residence time of 5 min. The authors found that the apparent porosity of the composite sample was 1.15% with 26.41 GPa of microhardness, 4.51 g/cm3 of apparent density, a friction coefficient of 0.54, and wear rate of $1.978 \times 10^{-6} \,\text{mm}^3/\text{Nm}$ [126]. Feng et al. prepared dense (Hf, Zr, Ti, Ta, Nb)B2 highentropy nano sized (300-500 nm) ceramics using the SPS method, during which they used stoichiometrically weighed powders of HfO₂, Ta₂O₅, TiO₂, ZrO₂, Nb₂O₅, B₄C, and carbon black. Three different formulations were performed for the synthesis of high entropy boride (HEB) ceramics using different quantities of Nb. Oxides were clubbed with an excess of B₄C and carbon. The powdered mixtures of HEB were synthesized initially for 3h under a moderate vacuum (~3 Pa) at 1,650°C using the boro/carbothermal reduction process. Subsequently, the HEB ceramics were subjected to a two-step SPS method under ~2 Pa of vacuum and at the highest temperature peak of 2,100°C. During the SPS process, an isothermal hold for 5 min, with a 15 MPa uniaxial pressure at 1,650°C was applied to remove the impurities which occurred in the form of remnant oxide [127]. Ensuring the certainty of the spatial uniformity of the sample properties is a major challenge usually encountered in an SPS process. Several studies have also shown that some differences and a non-uniform temperature gradient/distribution occur during SPS tooling. The non-uniform temperature gradient is observed between the average temperature of the sample and the outer surface of the die that is in contact with the thermocouple of the unit. It is primarily attributed to the non-uniform thermo-electric properties of the SPS tooling. The improvement in the uniformity of the temperature may be achieved via optimization. However, the application of SPS in sintering thermo-electric samples has uncovered an additional heat source and temperature gradient. Another point to consider is the loss or generation of the heat during the process by the Peltier effect. In certain instances, e.g., with samples such as nano sized boron carbide, it was found that when the sample was sintered at high temperatures of 2,000 K, a significant temperature gradient was observed between the top and bottom sides of the sample. The

temperature gradient causes severe loss and heterogeneity in its microstructure and mechanical properties. The contact surface of the specimen, graphite tooling, induction, and pulse frequency, also influence (or contribute to) a potent Peltier effect. A p-type conductor such as boron carbide and an n-type conductor such as graphite experiences punchthrough electron-hole recombination over the top surface of the specimen, thus generating an electron-hole pair at the bottom surface during the SPS process. This phenomenon causes the cooling of the bottom contacts and the heating of the top layer. Researchers have observed a decrease in polarity and thermal changes when AC is used instead of DC electric fields. Due to the Peltier effect, the nano boron carbide demonstrates erratic melting behavior. When the innate inhomogeneity is easily noticeable along with a lower relative density of the sample, the driving force and time eventually contribute to an increase in density by 100%. Additionally, the irregular grain size results from the non-uniform relative density, which can be avoided by introducing dielectric plates (such as alumina) between the sample and graphite punches to optimize the quality of the properties of the final product by removing the thermo-electric effects [128]. Nayebi et al. synthesized TiB₂-Ti₃AlC₂ ceramic composites at 1,900°C for 7 min using the SPS method at 30 MPa biaxial pressure [129]. Buinevich et al. fabricated ball milled and combustion synthesized non-stoichiometric nano structured hafnium carbonitrides (HfC_xN_y) which were further consolidated using the SPS method at a temperature of 2,000°C for 10 min under a constant pressure of 50 MPa [130]. Park et al. synthesized and studied the behavior of nano sized TaNbHfZrTi high-entropy alloy composites by the hydrogenation-dehydrogenation reaction at 1,100°C using the SPS method [131]. Jiang et al. studied the sintering behavior of the Ce₂Zr₃(MoO₄)₉ ceramics processed by the RS method and analyzed their vibrational spectra and microwave dielectric properties [132]. Sun et al. synthesized ball milled CaZrTi₂O₇-zirconolite based ceramics that were further consolidated by reactive SPS (Figure 9) for plutonium disposition application. The SPS synthesis was performed in the range of 900-1,450°C from 0.1-10 h, between 15 and 50 MPa of uniaxial pressure along with a solid-state reaction [133]. Rominiyi et al. studied the oxidation, microstructure, and tribological behavior of nano Ti-Ni-xTiCN ceramic composites by SPS [134].

2.4 HP and HIP

This process involves the application of a high-grade temperature (up to 2,200°C) and uniform directional pressure

Reactive Spark Plasma Sintering Sun et al (2018)

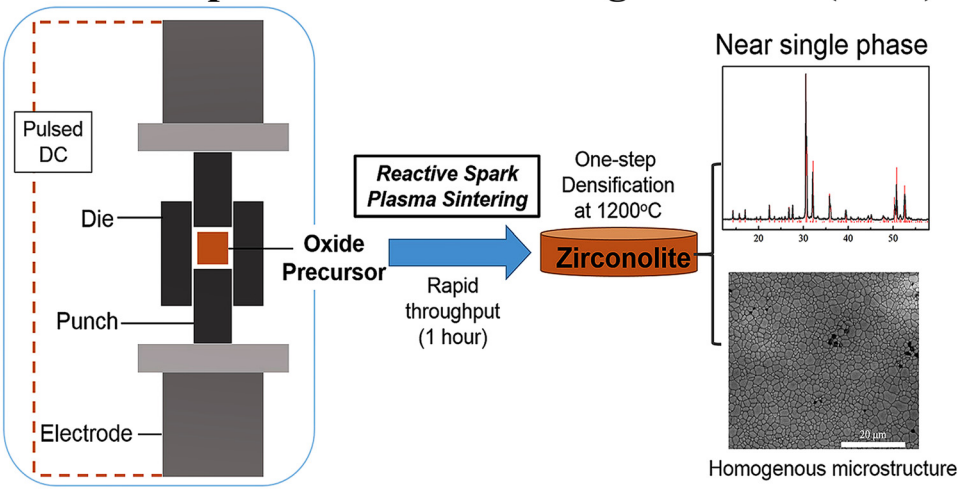


Figure 9: A generalized reaction spark plasma process scheme for the synthesis of Zirconolite and the obtained crystallinity and microstructure as reported by Sun *et al.* [133]. Reprinted with permission from Elsevier.

(200-500 MPa) on the material, simultaneously to elevate the densification and sintering of the UHTC material at a temperature that is much lower than the surrounding temperature. Due to the fast rate of the densification process, the grain size in the material is always maintained which improves the thermo-mechanical and thermal properties of the UHTC material. The process is commonly used in the production of ceramics, metals, and composite materials. Here are some advantages and disadvantages of HP: HP produces materials with high density, uniformity, reduced porosity, improved strength, and grain alignment. Few drawbacks of the process include high equipment and manufacturing cost and the process requires a significant amount of energy to heat the material. It also has limited shape complexity and material compatibility as it may not be suitable for all materials due to high pressure and temperature of the process. The process is also time-consuming which can limit its use in certain manufacturing applications. On the other hand, HIP involves utilizing high temperatures and pressures to condense metal or ceramic powders into solid materials. The advantages of HIP comprise better material properties, improved surface finish, customizable shapes, material variety, and reduced waste. Nevertheless, HIP has limitations such as high cost, time consumption, safety hazards to operators, as well as size and material thickness restrictions [135-137]. Kang et al., prepared an in situ micro and nano scaled W steel first by selective laser melting (SLM) followed by the HIP. The HIP process has a maximum limit of pressure (207 MPa) and temperature (2,000°C). The HIP was performed completely in a pure Ar atmosphere at 950°C with a cooling/heating

rate of 10°C/min, holding time of 120 min, and at a pressure of 150 MPa. During the post HIP process, it was found that the SLM samples exhibited a higher density without any change. The sample finally demonstrated a high yield strength of 1,025 MPa with an ultimate tensile strength between 980 and 1,470 MPa [138]. Sun *et al.* prepared a WTaMoNb/Cu nano composite with a stable microstructure using dual-step mechanical alloying and HP sintering [139]. Figure 10 shows the schematic illustrations of the HP and HIP processes, a step wise example for the HP synthesis of micro/nano SiC, and the basic difference between the HP and HIP processes [140,141,136,142].

Lozanov et al. prepared Ir-based ultrahigh-temperature intermetallic composites (MIr_{3+x}, where M = Hf, Ta) using the HP process. The powders were mixed and filled in a graphite die maintained at ~1 kPa in an Ar atmosphere at a pressure 110-130 kPa. The dies were pressed uniaxially at 20 MPa followed by heating at 2,073 K at a rate of 100 K/min with 20 min of exposure time at the peak temperature. Later, the chamber was cooled for 1h to reach temperatures between 323 and 343 K, respectively. The obtained samples demonstrated a thermal diffusivity between 11 and 13 mm²/c, thermal conductivity of approximately 39.4 W/m K at 1,700 K, heat capacity (C_p) of approximately 102.3 J/mol K at T = 298 K, CTE of approximately $5.2 \times 10^{-6} \text{ K}^{-1}$ between the temperatures of 300 and 1,100 K [74]. It is acknowledged that the preparation process of SiC heavily influences the chemistry and microstructure of the overall product thereby affecting the properties of the final product. Taking this factor into consideration, Šajgalík et al. prepared an additive-free ultra-high creep resistant SiC ceramic using rapid hot pressing. The

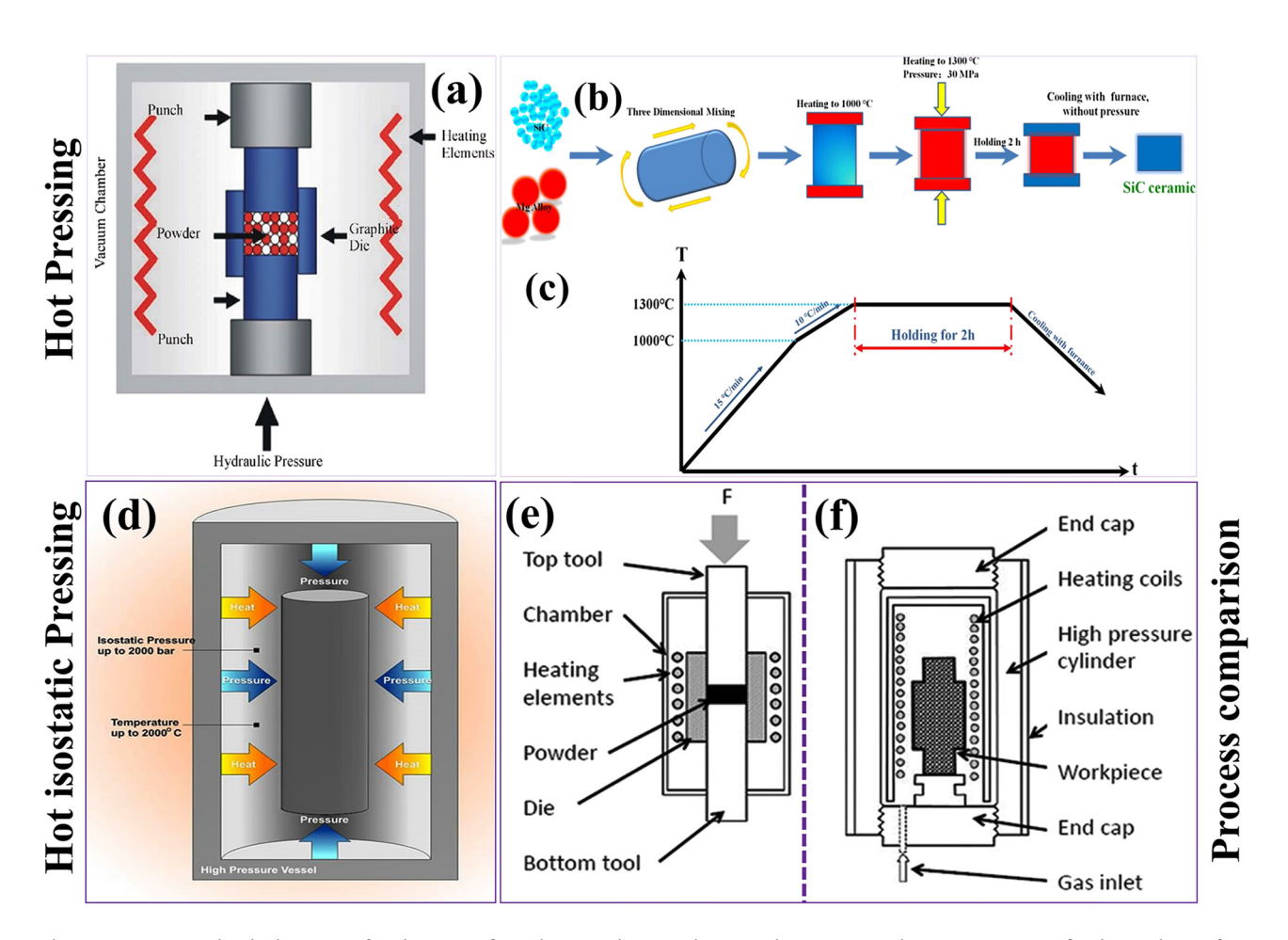


Figure 10: (a) Generalized schematics of HP by Moustafa *et al.* [140]; schematic diagrams demonstrating (b) sintering process for the synthesis of SiC ceramic by HP method and (c) the heating curve designed for the process by Li *et al.* [141]; (d) conventional HIP method [136]; schematic comparison between (e) HP and (f) HIP processes by Dobrzański *et al.* [142]. Reprinted with permission from (a) Scientific Research Publishers; (b and c) from Elsevier; (d) from the AZoNetwork; and (e and f) from IntechOpen Limited, United Kingdom.

researchers suggested that the β - α SiC phase transformation and the GB sliding controlled by GB diffusion are responsible for the creep mechanism at higher temperatures of 1,500–1,750°C and at compressive loads of 200–400 MPa [143].

Potanin *et al.* synthesized micro and nano sized MoSi₂–ZrB₂–SiC and MoSi₂–HfB₂–SiC composites using the combined synthesis of ball milling, combustion synthesis, and hot pressing. According to the researchers, the obtained composites have the potential to be used as high-temperature materials for industrial heaters. Powders of Mo, Hf, Zr, Si, amorphous B, and amorphous carbon black were mixed in the desired proportions and were mechanically activated in a planetary ball mill for 5 min at a speed of 700 rpm. The mixtures underwent combustion synthesis (self-propagating high-temperature synthesis; SHS) under an Ar atmosphere at 2 atm of pressure. The powders were subsequently ball milled. Thereafter, the powders were consolidated using HP under a pressure of 35 MPa at 1,600°C at a heating rate of 10°C/min for 10 min of isothermal exposure in a vacuum to

yield the final composite products. The obtained composites had a 97–98% relative density and an unreactive continuous oxide layer of crystalline α -quartz (a high-temperature alteration of SiO₂) formed which was strengthened with HfO₂, ZrSiO₄, ZrO₂, and HfSiO₄ precipitates. The composites had 2–3% of residual porosity, hardness of 12–14 GPa, strength of 350–400 MPa, and fracture toughness of 6.5–7.1 MPa m^{1/2}. The composites exhibited some weight gain when tested for their oxidation mechanism for 4 h at 1,650°C which is a characteristic of the *in situ* development of a dense protective layer [4].

Table 3 lists the modulus properties of the high-temperature silicide based nano refractory materials [51,60]. Vorotilo *et al.* synthesized both nano and micron sized ZrB₂–TaB₂–TaSi₂ mixed composite ceramics using both the SHS and HP methods. The powders of Zr, B, Ta, and Si were milled and later subjected to the SHS process and milled again to obtain a fine powder which was further consolidated by an HP process at 1,700°C for 10 min of

Table 3: Silicide based high temperature refractory materials and their modulus property [51,60]

Types of silicide material	Melting point (°C)	Density (g cm ⁻³)	Young's modulus (GPa)
ZrSi ₂	1,620	4.84	228
TaSi ₂	2,200	8.94	338
NbSi ₂	1,920-2,484	5.62-7.16	180-362.8
MoSi ₂	2,020-2,180	6.18-8.9	414-439
WSi ₂	2,160	9.69-9.86	438-467.9
HfSi ₂	1,700	7.92	227

exposure time under a pressure of 30 MPa. The obtained composite ceramic yielded a relative density of 95-98%, hardness (HV₁₀) of 19.2 GPa, and crack resistance (K_{1c}) of 3.5 MPa m^{1/2} [57]. The HIP process, in contrast, has an advantage over the SHS process because the samples are sintered at low temperatures for a short holding time. During consolidation, this prepares defect free sub-micro/ nano structured powdered materials with minimized grain growth. However, when the stress state is that of HIP conditions and a material has a lower shear viscosity, extremely small grain size, and a flattened pore, then the pore deforms, shrinks anisotropically, and finally disappears during the holding time. The pressure driven sintering usually involves several mechanisms including plastic yielding, and diffusional and power-law creep. When the stress levels are greater than the yield stress, there is a probability of macroscopic deformation, and the stress potential determines the power-law creep for the obtained porous material. However, when the stress levels are low, the diffusional creep becomes the prevailing deformation mechanism. Here the macroscopic strain rate is linear relative to the hydrostatic stress and thermodynamic operating force for pore shrinkage, which is the sintering stress. To predict shrinkage in the final product, the constitutive equations help to determine the densification mechanisms. Notably, during the densification process, the use of pressures higher than 100 MPa for HIP sintering becomes mandatory and it is crucial to completely remove the material defects such as cracks, large grain sizes, and growth, respectively. For decreasing the large pore size/ voids during the densification process with HIP, it is found that the use of very high pressures of more than 100 MPa sometimes do not alter or shrink the pore size because the time it takes to reach the reference density decreases, and it is inversely proportional to pressure. This renders the time dimensionless and excludes its consideration, thus, high pressures may be ineffective at reducing the large pore size during the HIP process [144]. Kaplanskii et al. synthesized and optimized a nano phased Ni₄₁Al₄₁Cr₁₂Co₆ alloy

powder using plasma-spheroidization in a plasma torch and layered the alloy on the turbine rotor blade models using laser synthesis (laser powder bed fusion-LPBF). The researchers investigated the HIP effect on the LPBF parts for their structural and thermo-mechanical properties. The LPBF parts were initially aged to ensure that the reinforced agents were well precipitated and well dispersed on the layers and have relaxed residual stress. Later the thermal treatment at 1,423 K was performed in a vacuum resistance furnace equipped with a W heating element under a vacuum of 1.3×10^{-5} Pa for 3 h of constant thermal exposure. Post thermal treatment, the blades were partially subjected to an HIP process at 145 MPa of pressure and at 1,523 K to decrease the porosity and remove the structural and property-based anisotropy. It was observed that HIP improved and significantly decreased plastic deformation, and the mechanical strength of the rotor blade at 85 K, developed by the combination of the LPBF, aging, and HIP process, was greater than that of the other fabricated (as-HIP and as-LPBF + aging) blades [145]. Lv et al. synthesized and fabricated a new CrMoNbWTi-C refractory high-entropy alloy composite which was co-strengthened using fine-grained intermetallics and UHTC carbides by mechanical alloying and the HP method between 1,400 and 1,450°C. The composite demonstrated a good elastic modulus (247.95 GPa), compressive fracture strength (3,094 MPa), and hardness (8.26 GPa) [146]. Recently, Herrmann and Räthel described the basic process and applications of HP and HIP in great detail [147].

2.5 Plasma/Physical vapor deposition (PVD) and Chemical vapor deposition (CVD)

The deposition techniques can efficiently coat good quantities of the UHTC material precisely onto the substrate or on any of the surfaces of the components. The plasma coating generally involves melting the precursor material in gas plasma before the material is transferred to and deposited under high velocity onto the targeted substrate, where the coating cools and solidifies. However, this process (plasma spraying) generates large amounts of defects in its coatings which could improve the thermal insulation resistance even when there are immediate changes in the temperature gradient. Additionally, the CVD process utilizes the benefit of the chemical reactions involving the gas and precursor materials to deposit the coating on the substrate directly (Figure 11) [148-152]. The coating material obtained by this process is always dense, flawless, and corrosion and oxidation resistant in comparison with the spray coating. In comparison, few merits and demerits are often found with the PVD/CVD, even though it is one of the preferred methods used for producing UHTCs which results in remarkable thermal stability and mechanical properties, making them suitable for high-temperature applications like aerospace and nuclear industries. PVD/ CVD provides UHTC materials with high purity, customizable composition, coating uniformity, and improved wear and corrosion resistance. However, the process is complex, costly, and requires skilled personnel and specialized equipment. The production capacity of PVD/CVD is limited due to the slow deposition rate, and the process can produce a rough surface finish, which may require additional processing steps to achieve the desired quality. Safety hazards such as high temperatures, vacuum environment, and hazardous chemicals must be mitigated with appropriate safety protocols and equipment [153]. He et al. synthesized high-temperature carbon/carbon (C/C) composites with SiC/pyrographitic carbon (PyC) coreshell structured nanowires using chemical liquid-vapor deposition (CLVD). The researchers used polycarbosilane (PCS) and SiC as the precursors and the preforms were made by punching a 2D needle into the carbon felt. The SiC nanowires and preforms were immersed in liquid xylene/PCS solution and pyrolyzed in the CLVD system at 950°C for 6 h, followed by heat treatment in Ar at a temperature range of 1,350-1,900°C for 2 h at a 10°C/min heating rate to yield the composites. The SiC/PyC coreshell structured nanowire composites were prepared by soaking the as-prepared SiC nanowire composites in xylene and then deposited using CLVD for 2 h at 950°C. At this stage the xylene is pyrolyzed into PyC and the PyC is gradually deposited onto the surface of the SiC nanowires leading to

the formation of SiC/PyC core—shell structure nanowire composites [154].

Ren et al. fabricated a C/C bi-phase coated with a HfC-ZrC composite using CVD to investigate the anti-ablative and anti-oxidative properties. The raw materials used for the synthesis were the C/C substrate and SiC sandpaper which were ultrasonically cleaned and dried, HfCl₄, ZrCl₄, CH₄, H₂, and Ar. The deposition was performed in a vertical tube furnace. The HfCl4 and ZrCl4 powders were initially mixed by ball milling, and loaded into the sublimation chamber and the C/C substrate was loaded into the reaction chamber. The deposition was performed between 1,200 and 1,350°C at 3 kPa in an inert Ar atmosphere under a gas flow for 2 h. Later, CH₄ and H₂ were cut down and cooled in Ar ambience to yield the C/C bi-phase coated HfC-ZrC composite. The following equations express the possible chemical reactions occurring during the deposition process (Eqs. (2)–(6)).

During deposition:

$$HfCl_{4(g)} + 2H_{2(g)} \rightarrow [Hf]_{(g)} + 4HCl_{(g)},$$
 (2)

$$ZrCl_{4(g)} + 2H_{2(g)} \rightarrow [Zr]_{(g)} + 4HCl_{(g)},$$
 (3)

$$CH_{4(g)} \rightarrow [C]_{(g)} + 2H_{2(g)},$$
 (4)

$$[Hf]_{(g)} + [C]_{(g)} \to HfC_{(s)},$$
 (5)

$$[Zr]_{(g)} + [C]_{(g)} \to ZrC_{(s)}.$$
 (6)

The composites were evaluated for their anti-ablation property for 60 s by oxyacetylene ablation, where it was discovered that the HfO₂ and ZrO₂ played an important role and there were sufficient grains on the surface for the formation of a strong oxide layer, which helped to

Schematic of CVD

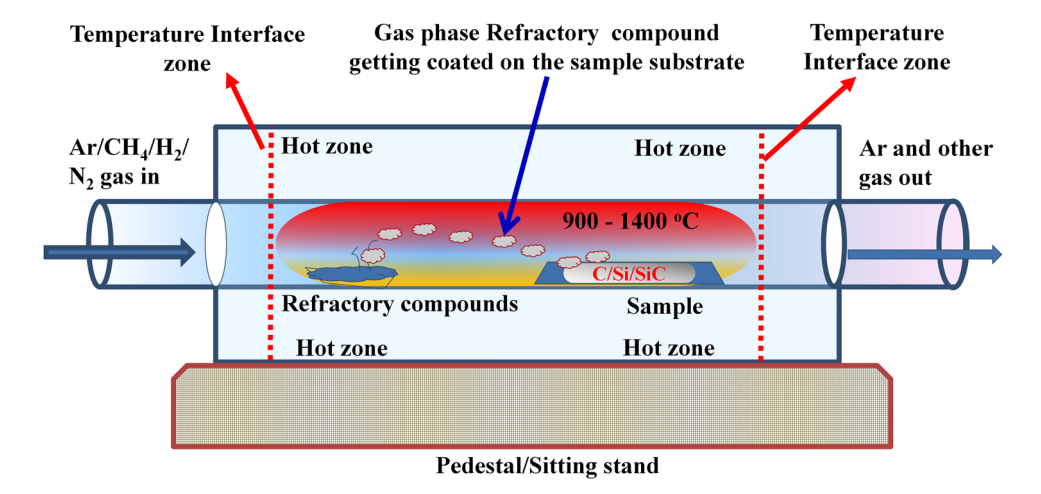


Figure 11: A generalized schematic of CVD process adapted and modified from Dhand et al. [149–152].

ensure negligible oxygen diffusion. Eqs. (7)–(12) express the reactions occurring during the ablation process.

During ablation:

$$HfC_{(s)} + 2O_{2(g)} \rightarrow HfO_{2(s)} + CO_{2(g)},$$
 (7)

$$2HfC_{(s)} + 3O_{2(g)} \rightarrow 2HfO_{2(s)} + 2CO_{(g)},$$
 (8)

$$ZrC_{(s)} + 2O_{2(g)} \rightarrow ZrO_{2(s)} + CO_{2(g)},$$
 (9)

$$2ZrC_{(s)} + 3O_{2(g)} \rightarrow 2ZrO_{2(s)} + 2CO_{(g)},$$
 (10)

$$HfO_{2(s)} \rightarrow HfO_{2(l)}, \tag{11}$$

$$ZrO_{2(s)} \rightarrow ZrO_{2(1)}.$$
 (12)

After the test it was found that the linear ablation rate ($R_{\rm l}$) and mass ablation rate ($R_{\rm m}$) of the composite coating was $-0.16~\mu m/s$ and 0.34~mg/s, respectively [155]. Temperature plays an important role in the deposition and microstructure control of the coating.

- The surface reaction controls the coating deposition at lower temperatures and crystal nucleation dominates during the deposition process that results in a smaller grain size of the coated material.
- 2) At high temperatures, the gas transmission controls the coating and deposition process, where the large grain crystal growth predominates in the coated material. With the increase in the surface temperature, the release of gases such as CO/CO2, saturated gas vapor pressure, followed by gas vaporization, and the production of voids within the oxide layer occurs. Due to a higher CTE of the carbide coating and oxide layers, excessive thermal stress and shock cause the coating to crack. Thus, the crack channels the diffusion of the oxidizing gas leading to rapid substrate and coating oxidation. During the post ablative stage, the rate of oxidation of the coating and the oxygen diffusion becomes greater due to the increase in the size of the cracks/voids, respectively. Additionally, this causes the coated oxide or melt material to lose its weight and thickness due to the high pressure/speed and mechanical abrasion inflicted by the ablation torch [142-152,154,155]. Tanaka et al. synthesized a highly ordered nanocomposite of cubic (B1)-TaC (111) and rhombohedral-Ta₃C₂(0001) phases over the Al₂O₃(0001) substrate using ultra-high vacuum DC magnetron sputtering of a thick TaC target under a vacuum of 5 mTorr in the presence of an Ar/C₂H₄ gas mixture. The reaction/deposition was performed at substrate temperatures of 1,123 and 1,273 K, respectively. The process involves 10 min of cleaning the Al₂O₃(0001) substrate with acetone, isopropanol, and distilled water using ultra-sonication, followed by drying under a stream of N2 and mounting on a heating stage, and transferring to the deposition chamber after evacuating the chamber below 10⁻⁸ Torr. In the

deposition chamber, the sample is thermally degassed at 1,273 K until the base pressure is $<6.0 \times 10^{-9}$ Torr. When the temperature is set to 1,123 or 1,273 K within the DC magnetron sputtering unit, TaC films are deposited for 2 h on the substrate in the presence of Ar and C_2H_4 gas mixtures at 5 mTorr of vacuum and at a deposition rate of 0.03 nm/s at 50 W of constant target power. The other parameters, such as variable current (0.15–0.16 A) and voltage (297–307 V) range, is followed up for creating TaC film during the reaction. Once the deposition is finished and the desired parameters attained, the heater is switched off, the samples are cooled, and analyzed [156].

Figure 12 depicts the general process of physical vapor deposition (PVD) using different types of magnetron (RF and DC types) sputtering to yield good quality coatings of the nano structured refractory materials onto the targeted substrate surface [157–159].

The PVD technique is useful because a wide variety of substrate materials, including alloys, ceramics, metals, glass, and polymers may be utilized. Additionally, PVD utilizes a very large scope of coating materials including alloys, metals, metal oxides, nitrides, and carbides. The process ensures a high-quality coating adhesion on the substrate with a refined microstructure based on a selection of suitable coating parameters (precursor composition, temperature, deposition rate, and film thickness). PVD is highly useful in opto-micro-electronic devices for superior quality thin film production, improved tribo-performance, anti-corrosion layering, thermal barrier, heat dissipators (sinks), and aesthetic coatings. Among the different types of available PVD methods, thermal evaporation is the most opted method due to its ease of operation and its ability to evaporate large varieties and quantities of materials. The versatility of the method helps to easily achieve the deposition of the desired material in the vapor phase under vacuum conditions (pressure < 5–10 torr) assisted by a resistive heater as the heating source. Thus, the transportation of the vapor atoms toward the low pressure zone helps in the deposition of the material onto the substrate aligned linearly from the source [160]. The formation of the desired fine-structured morphologies is a highly complex phenomenon because there is a contest between the surface transport effects and the depositing vapor flux during the deposition process. Thus, there is a two-fold challenge to optimize the parameters governing the PVD processing to obtain the desired microstructures. The primary challenge is selecting the spatial properties and the deposition conditions for the target to be deposited onto the substrate. The magnetron sputtering deposition parameters include, the gas/target/substrate composition,

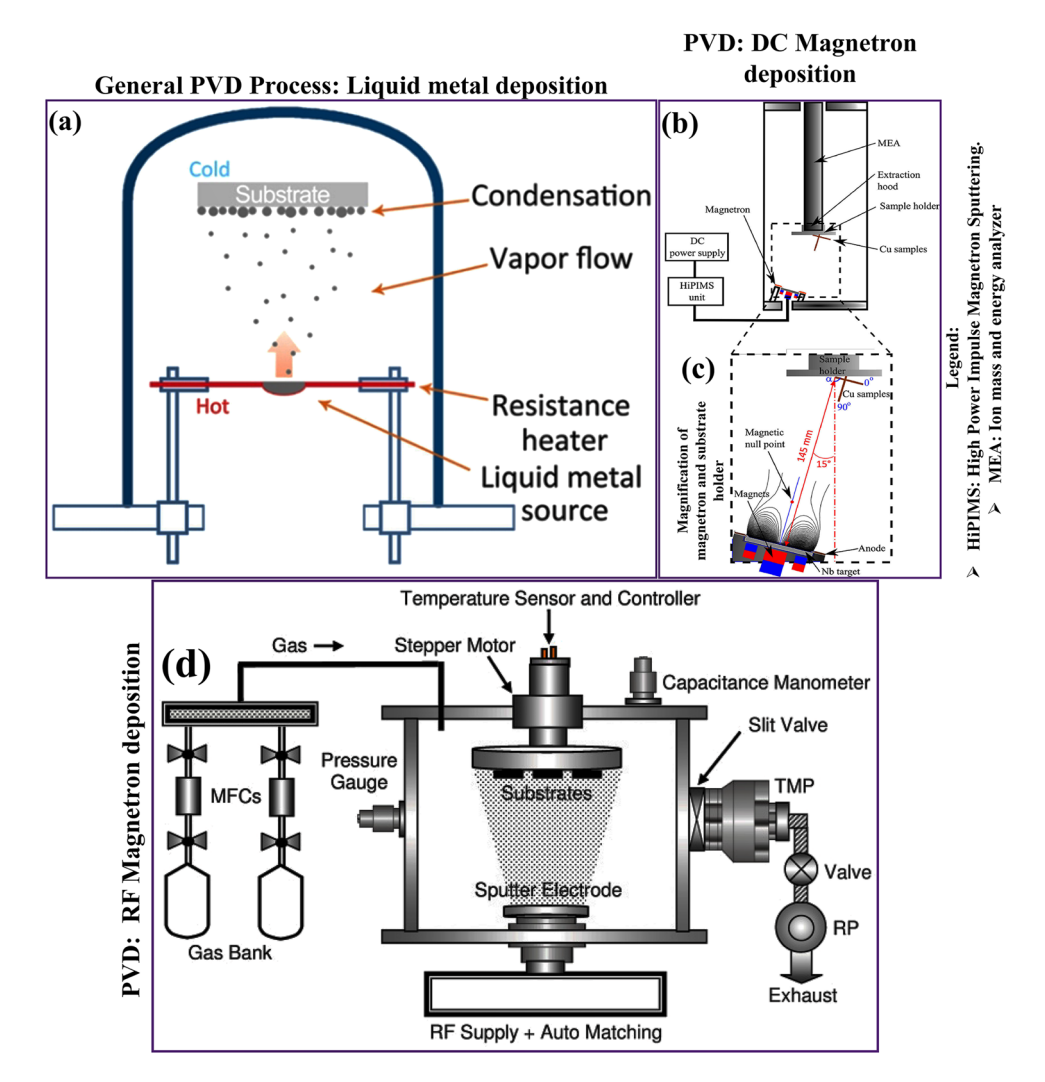


Figure 12: (a) Generalized schematic of physical vapor deposition (PVD) reaction involving the deposition of the liquefied metal source by Yu *et al.* [157]; schematic PVD diagram demonstrating (b) DC magnetron deposition unit; (c) magnified portions of the magnetron and the substrate holder within the chamber by Avino *et al.* (2020) [158]; (d) schematic diagram of PVD unit involving radio frequency (RF) based magnetron deposition unit by Kulkarni *et al.* [159]. Images (a–d): Reprinted with permission from Elsevier.

background pressure, temperature, and sputtering power. Likewise, the important properties for the deposition of the relevant materials are the atomic stoichiometry of the target species and the bulk/surface diffusion onto the substrate [161]. Kameneva *et al.* investigated improving the physicomechano-tribological properties, structural and phase transformations by using cathodic arc deposition (Arc-PVD) equipped with magnetron sputtered targets of Ti and Al for the synthesis of a nanostructured ${\rm Ti}_{1-x}{\rm Al}_x{\rm N}$ coating on a WC–Co substrate. The researchers also studied the effects on the composition and phase concentration of the nano-thick sized coating by controlling the temperature and deposition conditions on the surface of the cathode and substrate during the process [162]. Jokanović *et al.* fabricated multilayered nano thin films of titanium-

oxy-nitride and Cu-doped titanium nitride on a glass substrate using different PVD techniques and investigated its physico-chemical properties [163]. Kumar *et al.* deposited uniform nano TaC and SiC layers onto a graphite tube using the CVD method. Initially the authors synthesized tantalum chloride (TaCl₅) *in situ* by the chlorination of Ta chips at 550°C for 30 min. Later, a graphite tube was placed in the CVD chamber and TaC was deposited onto the tube due to the reduction reaction between TaCl₅ and CH₄ in the presence of H₂ gas at a pressure of 50–100 mbar and temperatures between 1,050 and 1,150°C. Similarly, another set of tubes was placed in the CVD chamber and SiC was deposited by introducing methyl-tri-chlorosilane and H₂ gas at 1,000°C and 50 mbar. The coating thickness at 1,150°C was approximately 600 and 400 μ m

at 1,050°C for the 10 h duration of the additional deposition. The samples were tested for their anti-ablation property for 120 s using an oxyacetylene flame. The results indicate that the coatings were intact without any change in their integrity albeit with a negligible amount of erosion. The analysis revealed the presence of nano aggregates of the surface oxide phases (TaO2, Ta2O5, and SiO2) of the TaC and SiC coatings, which is believed to have protected the underlying substrate from the high temperature of 2,000°C. The researchers suggested that these uniform CVD coatings on other geometrical objects/propulsion systems, including throat inserts, nozzles, and chambers of rocket motors, has potential which should be fulfilled in the coming years [164]. Zhu et al. performed both thermodynamic calculations and the synthesis of micro and nano mixed phases of ZrB₂ from a ZrCl₄–BCl₃–H₂–Ar system using CVD between 1,050 and 1,600°C at very low pressures [165]. Similarly, in their previous work, Zhu et al. performed an experimental synthesis using CVD accompanied by thermodynamic calculations for the production of a ZrC-SiC biphase from the ZrCl₄-C₃H₆-methyltrichlorosilane-H₂-Ar system using the FactSage thermochemical software [166]. Moraes et al. fabricated the sub-stoichiometric α-structured W-Ta-B thin films by PVD equipped with an in-house developed magnetron sputtering system. The researchers observed that the WB₂ thin films demonstrated an α-AlB₂prototype structure upon crystallization instead of their ω-W₂B_{5-z}-prototype structure, which is thermodynamically stable. By simulating the experiments using density functional theory (DFT), it was found that the stability of the α -WB₂ thin films is extremely regulated by point defects, such as vacancies, within the target PVD materials. The presence of α-TaB₂ and the phase transformation during the thermal decomposition reaction aids in the transformation of a- $W_{1-x}Ta_xB_{2-z}$ into a ω - W_2B_{5-z} -type structure when the temperatures are above 1,200°C. Experimentally, $W_{1-x}Ta_xB_{2-z}$ thin films were synthesized by the sputtering of TaB₂, WB₂, and carbon targets on the ultrasonically pre-cleaned steel foil or Si(100) substrates at a chamber temperature of 700°C (substrate temperature maintained at 400°C) and at a working pressure of 0.4 Pa. Throughout the experiments, the base pressure during the coating process was maintained below 3×10^{-4} Pa, target power varied between 0 and 11 W/cm² at 0.25 Hz of substrate holder rotation and bias voltage (-50 V) and the Ar etching of the targets in the deposition unit performed in an Ar atmosphere of 6 Pa with an applying voltage potential of -750 V for 10 min [167]. Startt et al. conducted a study to investigate the mechanical and thermal properties of MoNbTaTi quaternary refractory alloy across a broad compositional space using DFT simulations along with experimental validation. The study found

that there was good agreement between the simulation results and experimental data, which supports the use of DFT tools to predict properties of complex alloys. The first column of Figure 13 shows the thermodynamic properties calculated as a function of temperature for the equiatomic and experimental Ti-heavy (Ti34.7) composition using DFT under the quasi-harmonic approximations (QHA). The results were compared with the experimentally measured values for the Ti34.7 composition, which were obtained at approximately room temperature. Although there was some deviation between the DFT predictions and the experimental measurements, the modeling results were still quite close to the experimental values, indicating that the predictions of thermodynamic properties through both the harmonic and OHA are reliable [168].

In their study, Alvi et al. employed DFT simulations to determine the mechanical properties of the MoNbTaTi quaternary refractory alloy. The simulations revealed a Young's modulus value of 229 GPa, which agreed well with the experimental nanoindentation measurements. The researchers also observed that the high hardness observed in the metallic film could be attributed to the increased grain boundary strengthening resulting from the presence of nanocrystalline structure [169]. Dan et al. synthesized nano thin films of TiB₂/TiB(N)/Si₃N₄ deposited onto stainless steel (SS) substrates maintained at approximately 40°C by DC/RF magnetron sputtering. The researchers used TiB₂ and Si targets for the synthesis of the thin films. The substrates were chemically pre-cleaned and polished metallographically before deposition. The chamber was evacuated to a base pressure of 5.0×10^{-4} Pa. In the presence of Ar plasma, the TiB₂ layer developed and in an atmosphere of Ar and N₂, the Si₃N₄ and TiB(N) layers were deposited. The obtained TiB₂/ TiB(N)/Si₃N₄ thin film was tested for its photo-thermal conversion activity and the films exhibited 0.18 and 0.964 of emittance (at 82°C), and absorptance in the infrared region of 2.5–25 µm, and 0.3–2.5 µm in the solar spectrum range [170]. Table 4 lists the possible high-temperature refractory coating materials which can be coated on the surface of the C/SiC composites along with their melting points [171,172]. Table 5 lists the summarized melting points of a few inorganic refractory compounds and elemental metals which can be employed as high-temperature materials [171,172].

In this section we observe that the main factor for the deposition synthesis of the micro and nano phased refractory materials and their specific applications is based on the composite fabrication of the refractory matrix. The focus is also on the maintenance of a homogeneous microstructure for enhancing the thermal shock observed during the anti-ablation and oxidation tests. Very few research reports have so far been published regarding the

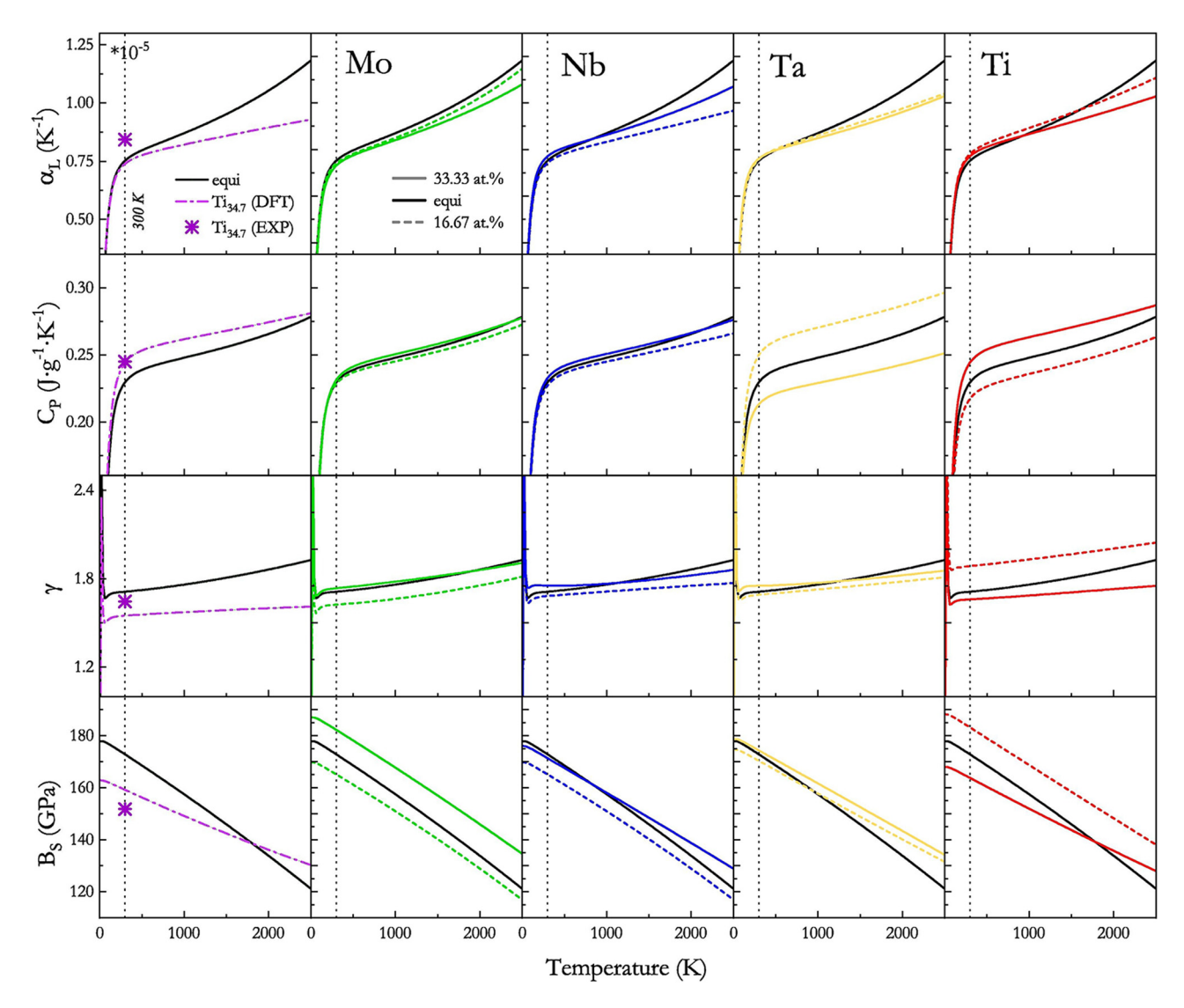


Figure 13: Thermodynamic properties of different compositions of the MoNbTaTi quaternary refractory alloy calculated using the QHA and density functional perturbation theory. The equiatomic composition is represented by a solid black line, while the Ti-heavy (Ti34.7) experimental composition is shown as purple dashed lines and cross points in the first column. Additionally, the thermal properties were calculated for one composition above (indicated by solid-colored lines) and below (represented by dashed-colored lines) the equiatomic composition for each element track. Reprinted from ref. [168], with permission from Elsevier.

preparation of other multi-functional composites using this method. Nevertheless, the fabrication and formulation of multi-functional composites comprising different mixtures and quantities of additives can produce diverse properties, such as superior thermal protection at higher temperatures, achievable full density, pore distribution, conditioned microstructures, enhanced thermo-physical attributes, and composite strength in the UHTC composites for their specific application. We have also noted that researchers have been modeling and simulating the parameters using FactSage, DFT, and other software to understand the effect on the synthesis, microstructure, and properties during the processing of the material composites. At present, a lot of attention

has been focused on the conservation of material architecture for the prospective growth and maturation of the highend C/C-UHTC composites for a desired set of properties and applications.

3 General applications

There are several high-temperature micro and nano structured materials that possess specific characteristics and properties which show potential for several applications. For example ZrB_2 is considered one such material, among

Table 4: Melting points of high-temperature refractory coatings on the surface of C/SiC composites [171,172]

Refractory compounds	Melting point (°C)	Refractory compounds	Melting point (°C)
TiO ₂	1,670	SiC	2,730
ZrO ₂	2,600-2,800	TiC	3,140
HfO ₂	2,900	TaC	3,985
HfB ₂	3,250	ZrC	3,530
TiB ₂	3,225	HfC	3,890
TaB ₂	3,037	Ta ₄ HfC ₅	4,215
ZrB_2	3,225	TiC + HfC	4,215

Data adapted with permission from Yang *et al.* [171] and Tkachenko *et al.* [172].

Table 5: Generally summarized melting points of inorganic refractory compounds and metals which can be employed as high-temperature materials [171,172]

General refractory compounds	Melting point (°C)	Elements	Melting point (°C)
Borides	1,960-3,250	W	3,410
Nitrides	1,900-3,300	Re	3,180
Silicides	1,540-2,400	Mo	2,620
Carbides	2,600-4,010	Nb	2,500
Oxides	250-2,900	Hf	2,222
Adapted with permiss	Ti	1,933	
[171] and Tkachenko 6	et al. [172]	Zr	1,855

other borides, which has a very good theoretical density and is highly stable above 2,000°C [173]. UHTC materials comprising variable nano constituents in ZrB₂/SiC and HfB₂/SiC have demonstrated their ability to be prospective candidates for re-entry vehicles as they are more often utilized in the sharp leading edges of the space crafts with passive cooling in the aerospace industry [174]. These materials are also found in other applications, including cutting tools, molten metal crucibles, electrodes for electrodischarge machining, wear resistant parts, electrical devices, Hall-Heroult cell, armor materials, rocket nozzles, divert/attitude control thrusters, reinforced cathode material for improvements in conductivity, aluminum evaporation boats, refractory parts, neutron shields in the nuclear sector, solar energy, high power-density microelectronics, and high-temperature structural parts [61,77,173,175,176]. The UHTC materials are still the same materials which were being studied and researched during 1950-1960 when the space revolution began [58,77,173]. It is necessary to expand and discover novel UHTC materials and explore their full potential for various applications. There is a high possibility that several other metallic nano-alloy compounds may not have been explored

for their UHTC properties and are yet to be discovered as potential materials in the evolution of high-end structural composites. There are existing opportunities in designing and formulating bi-phasic additions, which can render toughening by transformations in phase, suppress creep deformation at raised temperatures, enhance oxidation resistance, and densities [173]. The homogenized mixing, dispersion, dissolution, or diffusion of the nano phased additives into the UHTC matrix to form stable alloys can be manipulated at the crystal level to achieve the desired properties. All the researchers listed in the earlier sections have reported that their samples demonstrated good oxidation properties at moderate and higher temperatures when the samples were synthesized by the addition of TMs into their UHTC matrix. Furthermore, the nano additives also help strengthen the material against fracture both at ambient and raised temperatures. Computational methods offer an added advantage over the established experimental protocols, because there is a better chance of searching for and predicting novel UHTC materials based on their thermodynamic (entropy-stabilization) modeling. Perhaps other methods which have not been adopted thus far will also be utilized. Such formulations have potential to inspire the search for the novel UHTCs and other types of multi-functional materials [173]. As more UHTCs are discovered, they will provide more motivation and inevitably innovation shall occur for exploring prospective applications for UHTCs. During the last few years, nuclear applications have been considered due to serious accidents that were caused by the fuel, claddings, inert matrix fuels, non-oxide fuel pellets, moderators, and waste separation. From an environmental point of view, there is an urgent need to promote research and development for the use of UHTC materials as thermal and leak proof liners in the nuclear sector. However, the expected major challenges in this area are impurity minimization, cost affordability, dense material production, environmental hazards, shelf-life performance assessments, etc. [173]. Usually, most of the analysis and evaluation of UHTCs are done under normal pressures and temperatures but their applications are often performed at high temperatures of ≥2,000°C, or higher heat flux and in corrosive atmospheres. It is very unfortunate that such high-end research, analyses, and application evaluation of high grade UHTCs under extreme conditions are being performed only at classified or restricted laboratories because of homeland and defense security issues. The performance of UHTCs under extreme conditions is often deduced by the extrapolation of the data collected under ambient conditions, without considering the possible nonlinear behavioral trends generally caused due to creep, phase transformations, grain boundary softening, impurity phases, stress-affected micro-cracking, and sub-critical crack

development. Globally, there are very few established research laboratories which have the capability to evaluate materials under extreme conditions, including Missouri University of Science and Technology, Imperial College London, Indian National Aerospace and Defense Laboratories, University of Birmingham, Harbin Institute of Technology, NASA Ames Research Center, Korea Institute of Materials Science, and University of Arizona [173]. No doubt, it is a major challenge to maintain and sustain the extreme conditions in test facilities, especially when the sample is being tested under mixed environments. Essentially, at these extreme conditions most of the sensors are rendered in-operable; therefore, it is very difficult to obtain the actual data based on the material response. Hence, based on the above listed inputs, there is an urgent need to overcome these challenges by further research into the synthesis, development, maturation, property tailoring, and application realms of UHTC materials under extreme conditions.

4 Conclusion

In the present review, we have generalized and listed the characteristics of the nano UHTC/refractory compounds which belong to the family of materials that have very high melting points (>2,000°C), beneficial chemo-thermal stability, high strength, and hardness at elevated temperatures. We have listed the types of high-temperature metals, production issues, and applications along with their standard processing/synthesis routes. In summary, there are very few high-temperature materials such as SiC, oxide ceramics, Si₃N₄, and other nanocomposites of these materials that are structurally stable under oxidizing conditions. Of these refractory materials, the Si-derived nanocomposites have a maximum stability limit only to temperatures up to 1,700°C during the start (onset) of the oxidation process or have lower maximum stability temperatures when under a water vapor-based environment. Therefore, there is a need to design structural refractory materials that can tolerate oxidation and maintain their integral stability under extreme environmental and thermal conditions. In general, most of the carbides, borides, silicides, and nitrides of the transitional group metals are considered UHTC materials, but the focus is placed upon certain group IV-V elements including Zr, Ti, Ta, and Hf and their compounds due to their extremely high melting points and ability to withstand higher temperature environments by forming protective oxide nano layers. Due to such advantageous thermal properties, these materials are promising candidates in several high-temperature structural applications such as space and hypersonic vehicles, engines, plasma arc electrodes, furnace elements, cutting tools, and high-temperature shields. The synthesis and consolidation of thermo-resistant nanoalloys can be challenging due to the complexity of the process and the properties of the materials involved. Thermo-resistant nanoalloys are composed of two or more metallic elements that form a solid solution at the nanoscale, and their properties depend on the composition, size, and structure of the particles. One of the main issues with the synthesis of thermo-resistant nanoalloys is the difficulty in controlling the size and composition of the nanoparticles. This is due to the high reactivity of the metallic elements and the complex interactions between them during the synthesis process. Various synthesis methods have been utilized as listed in the previous sections, but each method has its limitations and may lead to poor stability and reproducibility. Similarly, the consolidation of thermo-resistant nanoalloys into useful forms can also be challenging. The consolidation process involves transforming the nanoparticles into a bulk material, which can be in the form of a powder, a thin film, or a bulk material. The main challenges of consolidation are related to the difficulty in maintaining the nanostructure and the homogeneity of the composition. Conventional consolidation techniques such as sintering or HP can lead to grain growth and segregation, resulting in poor stability and reduced thermo-resistant properties. Despite these challenges, thermo-resistant nanoalloys have a wide range of potential applications, such as in aerospace, energy, and biomedical fields as previously discussed. They can be used as high-temperature coatings, catalysts, or heat exchangers. In order to overcome the limitations of synthesis and consolidation, researchers are exploring novel approaches such as SPS, electrospinning, and additive manufacturing, which offer better control over the size, composition, and structure of the materials. Authors believe that based on this review, there should be a need for the development of novel synthesis techniques, which can offer precise control over the particle size, composition, and structure of the nanoalloys, resulting in improved performance. Additionally, more focus should be given in the area of optimization of alloy composition to enhance their thermal stability, mechanical strength, and oxidation resistance using high temperature additives like carbides, borides, silicides, and nitrides of W, Mo, Zr, Ti, Ta, and Hf into hetero metal-based systems that can significantly improve their high-temperature performance. On the basis of consolidation techniques, more improvement is needed to produce highly dense and uniform nanoalloys with improved thermo-mechanical and anti-corrosive properties. The future aspects can be focused more on investigation of new alloy compositions. Researchers could investigate the potential of using other elements or combinations of elements to further enhance the properties of these materials by using new synthesis techniques. Finally, it is important to evaluate the performance of thermo-resistant nanoalloys under extreme conditions, such as high radiation, extreme pressure, and corrosive environments. This could provide valuable insights into the potential of these materials for various applications. Moreover, UHTCs with moderate physico-chemical attributes are also gaining hold in present day high-end applications. As we have seen in this review, ZrB2-based composite ceramics have demonstrated their ability to form a protective oxide layer and have anti-ablative properties at very high temperatures; therefore, they can be applied in areas such as metal-molten crucibles, hypersonic vehicles, and high-temperature electrodes. However, they are poor in their mechanical capacity and ability to be sintered for specific applications due to their brittle nature which limits their use in the aerospace vehicle industry. Further in this review, we have listed and discussed various processing/ synthesis routes which help to improve the overall characteristics of different UHTC materials and the different additives including nano structured inorganic oxides and the use of C/C fiber based fabric [177]. Among the processing routes, sintering plays a major role either for direct synthesis or consolidating the material. Although SPS technology demonstrated several merits in the synthesis and development of various conventional and novel materials, there is a need for rapid development in understanding the cardinal process mechanisms (microscopic level), regular improvement in materials with a high sintering ability, high-temperaturetolerant dies, increase in the power of equipment for the quick construction of an automated production unit with excellent performance, development of more precise protocols, and methods for evaluating the performance testing standards of other SPS processed/synthesized materials [178]. There are several literature reports published on the challenges in anti-oxidation (protection) and the need for improving the resistance of nano carbon fiber reinforced SiC composites (C/SiC) against oxidation. Other advanced processes, such as coating the surface using CVD, PVD, and slurry methods, are found to be more suitable in improving the oxidation behavior of the micro and nano composite. Materials such as borides, carbides, oxides, silicide, and their combinations were found to be effective and predominantly used as coating materials on the surface of C/SiC composites. Of these combinations, boride/carbides were the most promising candidates, where multilayered coatings exhibit the best anti-oxidation performance results in various applications per-se. Nevertheless, a major drawback in these composites is the thermal coefficient expansion which is of great concern and attempts should be made for its

improvement. Moreover, research should also focus on the optimization and control over the multilayer uniform coating processes using different technologies applicable on larger surface area, evaluation of anti-oxidation behavior of C/SiC composites at temperatures greater than 1,800°C, and in different environments, such as under high humidity [171]. The authors believe that the stimulation of novel techniques and processes in improving the performance of the UHTC refractory materials under extreme conditions will keep inspiring and motivating researchers across the globe to produce near perfect materials for high-end application in several industrial sectors. As discussed earlier, the focus on synthesis, treatments, densification, stability, structural integration maintenance, inter-relational property enhancement, and anti-ablative and anti-oxidation performance improvements should be further explored. Other reinforced novel additives/filler nano materials should also be tested to evaluate their properties, along with simulation and modeling to guide in the fabrication of near perfect new materials with superior properties under extreme conditions. It is perceived, that by 2022–2030 the new wave in HTC research may enable active developments for the next three decades in producing new category stable materials for commercial grade applications. This will pave the way for more applied research opportunities and funding in basic research fields with industrial cooperation. Thus, it is very important for researchers globally to continue exploring new applications and property boundaries of UHTC materials from laboratory scale to practical world applications.

Funding information: This study was funded by the Basic Science Research Program under contract number 2020R1I1A3071046 (S. Kim) through the National Research Foundation of Korea (NRF) grant funded by the Ministry of Education (Korea) and supported by the Chonnam National University (Smart Plant Reliability Center) grant funded by the Ministry of Education (2020R1A6C101B197).

Author contributions: All authors have accepted responsibility for the entire content of this manuscript and approved its submission.

Conflict of interest: The authors state no conflict of interest.

References

[1] Routschka G, Granitzki KE. Refractory materials-ceramics. Digital Encyclopedia of applied physics. Weinheim, Germany: Wiley-VCH Verlag GmbH & CoKGaA; 2003. doi: 10.1002/3527600434.eap392.

- [2] ISO 836:2001-Terminology for refractories 2001:144. https://www. iso.org/standard/5205.html accessed December 5, 2020.
- [3] ISO 528:1983(en). Refractory products Determination of pyrometric cone equivalent (refractoriness) 1983:5. https://www.iso.org/standard/4596.html accessed December 5, 2020.
- [4] Potanin AY, Astapov AN, Rupasov SI, Vorotilo S, Kochetov NA, Kovalev DY, et al. Structure and properties of MoSi2–MeB2–SiC (Me = Zr, Hf) ceramics produced by combination of SHS and HP techniques. Ceram Int. 2020;46:28725–34. doi: 10.1016/j.ceramint. 2020.08.033.
- [5] Das Gupta S, Johar S, Jacobs JK, Das Gupta G. Heating elements and electrically conducting ceramics. Key Eng Mater. 1996;122–124:279–82. doi: 10.4028/www.scientific.net/kem.122-124.279.
- [6] Chakraborty SP, Banerjee S, Sharma IG, Suri AK. Development of silicide coating over molybdenum based refractory alloy and its characterization. J Nucl Mater. 2010;403:152–9. doi: 10.1016/j. inucmat.2010.06.014.
- [7] Das P, Paul S, Bandyopadhyay PP. Tribological behaviour of plasma sprayed diamond reinforced molybdenum coatings. Int J Refract Met Hard Mater. 2019;78:350–9. doi: 10.1016/j.ijrmhm. 2018.10.015.
- [8] Kentheswaran V, Dine S, Vrel D, Couzinié JP, Dirras G. Synthesis of nanometric refractory alloys powders in the Mo-Nb-W system. J Alloys Compd. 2016;679:80–7. doi: 10.1016/j.jallcom.2016.03.271.
- [9] Hoseinpur A, Jalaly M, Sh, Bafghi M, Vahdati Khaki J, Sakaki M. The effect of preliminary mechanical activation on the zinc loss control in combustive reduction of MoO₃ by Zn. Int J Refract Met Hard Mater. 2016;54:251–9. doi: 10.1016/j.ijrmhm.2015.08.002.
- [10] Nersisyan HH, Lee JH, Won CW. A study of tungsten nanopowder formation by self-propagating high-temperature synthesis. Combust Flame. 2005;142:241–8. doi: 10.1016/j.combustflame. 2005.03.012.
- [11] Braun J, Kaserer L, Stajkovic J, Leitz KH, Tabernig B, Singer P, et al. Molybdenum and tungsten manufactured by selective laser melting: Analysis of defect structure and solidification mechanisms. Int J Refract Met Hard Mater. 2019;84:104999. doi: 10.1016/j. ijrmhm.2019.104999.
- [12] Müller AV, Schlick G, Neu R, Anstätt C, Klimkait T, Lee J, et al. Additive manufacturing of pure tungsten by means of selective laser beam melting with substrate preheating temperatures up to 1000°C. Nucl Mater Energy. 2019;19:184–8. doi: 10.1016/j.nme. 2019.02.034.
- [13] Terentyev D, Xiao X, Lemeshko S, Hangen U, Zhurkin EE. High temperature nanoindentation of tungsten: Modelling and experimental validation. Int J Refract Met Hard Mater. 2020;89:105222. doi: 10.1016/j.ijrmhm.2020.105222.
- [14] Adil S, Suraj MV, Pillari LK, Sridar S, Nagini M, Pradeep KG, et al. On the effect of Fe in L12 strengthened Al–Co–Cr–Fe–Ni–Ti complex concentrated alloy. Materialia. 2020;14:100909. doi: 10.1016/j.mtla.2020.100909.
- [15] Rieger T, Joubert JM, Laurent-Brocq M, Perrière L, Guillot I, Couzinié JP. Study of the FCC + L12 two-phase region in complex concentrated alloys based on the Al-Co-Cr-Fe-Ni-Ti system. Materialia. 2020;14:100905. doi: 10.1016/j.mtla.2020.100905.
- [16] Jain R, Jain A, Rahul MR, Kumar A, Dubey M, Sabat RK, et al. Development of ultrahigh strength novel Co-Cr-Fe-Ni-Zr quasiperitectic high entropy alloy by an integrated approach using experiment and simulation. Materialia. 2020;14:100896. doi: 10.1016/j.mtla.2020.100896.

- [17] Fernandes CM, Senos AMR, Vieira MT. Control of eta carbide formation in tungsten carbide powders sputter-coated with (Fe/ Ni/Cr). Int J Refract Met Hard Mater. 2007;25:310–7. doi: 10.1016/j. ijrmhm.2006.07.004.
- [18] Du HL, Datta PK, Gray JS, Strafford KN. Sulphidation behaviour of FeCoCrAlY alloys containing refractory metals. Corros Sci. 1994;36:99–112. doi: 10.1016/0010-938X(94)90112-0.
- [19] Lech S, Polkowski W, Polkowska A, Cempura G, Kruk A. Multimodal discontinuous reaction in Ni–Fe–Cr–Al alloy. Scr Mater. 2021;194:113657. doi: 10.1016/j.scriptamat.2020.113657.
- [20] Polkowska A, Lech S, Bała P, Polkowski W. Microstructure and mechanical properties of Ni–Fe–Cr–Al wrought alumina forming superalloy heat-treated at 600–1100°C. Mater Charact. 2021;171:110737. doi: 10.1016/j.matchar.2020.110737.
- [21] Agca C, Neuefeind JC, McMurray JW, Liu J, Benmore CJ, Weber RJK, et al. In situ high-temperature synchrotron diffraction studies of (Fe,Cr,Al)₃O₄ spinels. Inorg Chem. 2020;59:5949–57. doi: 10.1021/acs.inorgchem.9b03726.
- [22] Terrani KA, Zinkle SJ, Snead LL. Advanced oxidation-resistant iron-based alloys for LWR fuel cladding. J Nucl Mater. 2014;448:420–35. doi: 10.1016/j.jnucmat.2013.06.041.
- [23] Stonic RH. Graphite as a refractory. J Am Ceram Soc. 1933;16:96–6. doi: 10.1111/j.1151-2916.1933.tb19202.x.
- [24] Gugliani G, Pal SK, Sen A, Prasad B. Development of a zirconiagraphite refractory for a SEN application. InterCeram Int Ceram Rev. 2014;63:136–40. doi: 10.1007/bf03401049.
- [25] Shen K, Chen X, Shen W, Huang ZH, Liu B, Kang F. Thermal and gas purification of natural graphite for nuclear applications. Carbon N Y. 2021;173:769–81. doi: 10.1016/j.carbon.2020.11.062.
- [26] Lang S, Drück H, Bestenlehner D. Ultrahigh temperature thermal insulation. Ultra-high temperature thermal energy storage, transfer and conversion. United Kingdom: Woodhead Publishing; 2021. p. 201–19. doi: 10.1016/b978-0-12-819955-8.00008-9.
- [27] Remyamol T, Gopi R, Ajith MR, Pant B. Porous silicon carbide structures with anisotropic open porosity for high-temperature cycling applications. J Eur Ceram Soc. 2021;41:1828–33. doi: 10.1016/j.jeurceramsoc.2020.10.060.
- [28] Park YH, Hinoki T, Kohyama A. Development of multi-functional NITE-porous SiC for ceramic insulators. J Nucl Mater. 2009;386–388:1014–7. doi: 10.1016/j.jnucmat.2008.12.202.
- [29] Cheng T. Ultra-high-temperature mechanical behaviors of twodimensional carbon fiber reinforced silicon carbide composites: Experiment and modeling. J Eur Ceram Soc. 2021;41:2335–46. doi: 10.1016/j.jeurceramsoc.2020.11.057.
- [30] Taneja K, Kumar M, Mahajan SB. Reaction mechanism for pressureless sintering silicon carbide boron carbide composite. Mater Today Proc. 2020. doi: 10.1016/j.matpr.2020.08.320.
- [31] Raju M, Sen S, Sarkar D, Jacob C. Synthesis of 3C-silicon carbide 1D structures by carbothermal reduction process. J Alloys Compd. 2021;857:158243. doi: 10.1016/j.jallcom.2020.158243.
- [32] Ramaswamy P, Tilleti P, Bhattacharjee S, Pinto R, Avijit Gomes S. Synthesis of value added refractories from aluminium dross and zirconia composites. Mater Today Proc. 2019;22:1264–73. doi: 10.1016/j.matpr.2020.01.419.
- [33] Khattab RM, Hanna SB, Zawrah MF, Girgis LG. Alumina-zircon refractory materials for lining of the basin of glass furnaces: Effect of processing technique and TiO₂ addition. Ceram Int. 2015;41:1623–9. doi: 10.1016/j.ceramint.2014.09.100.
- [34] Kumar P, Nath M, Ghosh A, Tripathi HS. Enhancement of thermal shock resistance of reaction sintered mullite-zirconia composites

in the presence of lanthanum oxide. Mater Charact. 2015;101:34-9. doi: 10.1016/j.matchar.2015.01.004.

DE GRUYTER

- [35] Roy J, Chandra S, Maitra S. Nanotechnology in castable refractory. Ceram Int. 2019;45:19-29. doi: 10.1016/j.ceramint.2018.09.261.
- [36] Spirig JV, Ramamoorthy R, Akbar SA, Routbort JL, Singh D, Dutta PK. High temperature zirconia oxygen sensor with sealed metal/metal oxide internal reference. Sens Actuators B: Chem. 2007;124:192-201. doi: 10.1016/j.snb.2006.12.022.
- [37] Suresh Kumar R, Sivakumar D, Venkateswarlu K, Gandhi AS. Mechanical behavior of molybdenum disilicide reinforced silicon carbide composites. Scr Mater. 2011;65:838-41. doi: 10.1016/j. scriptamat.2011.07.043.
- Rastogi RS, Vankar VD, Chopra KL. The effect of oxygen impurity on growth of molybdenum disilicide and its distribution during rapid thermal annealing of co-sputtered MoSi, thin films. Thin Solid Films. 1992;213:45-54. doi: 10.1016/0040-6090(92)90473-O.
- Jain MK, Das J, Deb S, Subrahmanyam J, Ray S. Analysis of residual thermal stresses in MoSi₂ based laminated composites. Int I Refract Met Hard Mater. 2017;68:9-18. doi: 10.1016/j.ijrmhm.2017. 06.002.
- [40] Guan S, Liang H, Liu Y, Lin W, He D, Peng F. Production of silicon carbide reinforced molybdenum disilicide composites using highpressure sintering. Ceram Int. 2020;46:23643-50. doi: 10.1016/j. ceramint.2020.06.137.
- [41] Mileiko ST, Kolchin AA, Galyshev SN, Shakhlevich OF, Prokopenko VM. Oxide-fibre/molybdenum-alloy-matrix composites: A new way of making and some mechanical properties. Compos Part A Appl Sci Manuf. 2020;132:105830. doi: 10.1016/j. compositesa.2020.105830.
- Barbi GB, Mari CM. Electrochemical kinetics of the water reduc-[42] tion at strontium doped lanthanum chromite (SDLC)/Yttria stabilized zirconia interfaces at high temperature. Solid State Ionics. 1983;9-10:979-87. doi: 10.1016/0167-2738(83)90119-4.
- [43] Rida K, Benabbas A, Bouremmad F, Peña MA, Sastre E, Martínez-Arias A. Effect of calcination temperature on the structural characteristics and catalytic activity for propene combustion of sol-gel derived lanthanum chromite perovskite. Appl Catal A Gen. 2007;327:173-9. doi: 10.1016/j.apcata.2007.05.015.
- Shevchik AP, Suvorov SA. Microstructure of refractories with participation of lanthanum chromite. Refract Ind Ceram. 2009:50:266-72. doi: 10.1007/s11148-009-9198-4.
- Pillis MF, Ramanathan LV. High temperature oxidation resistance [45] of rare earth chromite coated Fe-20Cr and Fe-20Cr-4Al alloys. Mater Res. 2007;10:279-82. doi: 10.1590/S1516-14392007000300011.
- Setz LFG, Santacruz I, León-Reina L, De La Torre AG, Aranda MAG, Mello-Castanho SRH, et al. Strontium and cobalt dopedlanthanum chromite: Characterisation of synthesised powders and sintered materials. Ceram Int. 2015;41:1177-87. doi: 10.1016/j. ceramint.2014.09.046.
- [47] Zupan K, Marinšek M, Novosel B. Combustible precursor behaviour in the lanthanum chromite formation process. Mater Tehnol. 2011;45:439-45.
- Toperesu PM, Kale GM, Daji J, Parkinson D. Development and [48] evolution of a novel (Zr_{1-x}Sn_x)O₂ toughened alumina-mullite slip cast refractory: Effect of SnO₂. J Eur Ceram Soc. 2021;41:2134-44. doi: 10.1016/j.jeurceramsoc.2020.10.070.
- Mora-Gómez J, García-Gabaldón M, Ortega E, Sánchez-Rivera MJ, Mestre S, Pérez-Herranz V. Evaluation of new ceramic electrodes based on Sb-doped SnO₂ for the removal of emerging

- compounds present in wastewater. Ceram Int. 2018;44:2216-22. doi: 10.1016/j.ceramint.2017.10.178.
- [50] Abdollahi M, Nilforoushan MR, Maleki Shahraki M, Chermahini MD, Moradizadeh M. The degradation behavior of highvoltage SnO₂ based varistors sintered at different temperatures. Ceram Int. 2020;46:11577-83. doi: 10.1016/j.ceramint.2020.01.186.
- [51] Mitra R. Mechanical behaviour and oxidation resistance of structural silicides. Int Mater Rev. 2006:51:13-64. doi: 10.1179/ 174328006X79454
- [52] Potanin AY, Pogozhev YS, Levashov EA, Novikov AV, Shvindina NV, Sviridova TA. Kinetics and oxidation mechanism of MoSi₂-MoB ceramics in the 600-1200°C temperature range. Ceram Int. 2017;43:10478-86. doi: 10.1016/j.ceramint.2017.05.093.
- [53] Mallik M, Kailath AJ, Ray KK, Mitra R. Electrical and thermophysical properties of ZrB2 and HfB2 based composites. J Eur Ceram Soc. 2012;32:2545-55. doi: 10.1016/j.jeurceramsoc.2012.02.013.
- Mallik M, Ray KK, Mitra R. Oxidation behavior of hot pressed ZrB₂-[54] SiC and HfB₂-SiC composites. J Eur Ceram Soc. 2011;31:199–215. doi: 10.1016/j.jeurceramsoc.2010.08.018.
- [55] Zhang L, Tong Z, He R, Xie C, Bai X, Yang Y, et al. Key issues of MoSi₂-UHTC ceramics for ultra high temperature heating element applications: Mechanical, electrical, oxidation and thermal shock behaviors. J Alloys Compd. 2019;780:156-63. doi: 10.1016/j. jallcom.2018.11.384.
- [56] Fahrenholtz WG, Hilmas GE, Talmy IG, Zaykoski JA. Refractory diborides of zirconium and hafnium. J Am Ceram Soc. 2007;90:1347-64. doi: 10.1111/j.1551-2916.2007.01583.x.
- Vorotilo S, Levashov EA, Petrzhik MI, Kovalev DY. Combustion [57] synthesis of ZrB2-TaB2-TaSi2 ceramics with microgradient grain structure and improved mechanical properties. Ceram Int. 2019;45:1503-12. doi: 10.1016/j.ceramint.2018.10.020.
- Wuchina E, Opila E, Opeka M, Fahrenholtz W, Talmy I. UHTCs: Ultra-high temperature ceramic materials for extreme environment applications. Electrochem Soc Interface, 2007;16:30-6. doi: 10.1149/2.f04074if.
- [59] Mubina S, Khanra AK, Saha BP. Enhancement of oxidation resistance of CVD SiC coated Cf/C-SiC hybrid composite tubes processed through Si-infiltration. J Alloys Compd. 2020;826:154107. doi: 10.1016/j.jallcom.2020.154107.
- [60] Vorotilo S, Potanin AY, Iatsyuk IV, Levashov EA. SHS of Silicon-Based Ceramics for the high-temperature applications. Adv Eng Mater. 2018;20:1800200. doi: 10.1002/adem.201800200.
- [61] Golla BR, Mukhopadhyay A, Basu B, Thimmappa SK. Review on ultra-high temperature boride ceramics. Prog Mater Sci. 2020;111:100651. doi: 10.1016/j.pmatsci.2020.100651.
- [62] Opila E, Levine S, Lorincz J. Oxidation of ZrB2- and HfB2-based ultra-high temperature ceramics: Effect of Ta additions. J Mater Sci. 2004;39:5969–77. doi: 10.1023/B:JMSC.0000041693.32531.d1.
- [63] Velappan S, Nivedhita P, Vimala R, Raja S. Role of nano titania on the thermomechanical properties of silicon carbide refractories. Ceram Int. 2020;46:25921-6. doi: 10.1016/j.ceramint.2020.07.077.
- [64] Mukhopadhyay S, Sen S, Maiti T, Mukherjee M, Nandy RN, Sinhamahapatra BK. In situ spinel bonded refractory castable in relation to co-precipitation and sol-gel derived spinel forming agents. Ceram Int. 2003;29:857-68. doi: 10.1016/S0272-8842(03) 00028-2.
- [65] Aarthi U, Babu KS. Grain boundary space charge modulation in $BaZr_{0.8}Y_{0.2-x}MxO_{3-\delta}$ with transition metal (M = Ni, Co, Fe, and Zn) co-doping. Int J Hydrogen Energy. 2020;45:29356-66. doi: 10.1016/j.ijhydene.2020.07.207.

- [66] Kim JW, Shim JH, Ahn JP, Cho YW, Kim JH, Oh KH. Mechanochemical synthesis and characterization of TiB $_2$ and VB $_2$ nanopowders. Mater Lett. 2008;62:2461–4. doi: 10.1016/j.matlet. 2007.12.022.
- [67] Gupta SK, Mao Y. A review on molten salt synthesis of metal oxide nanomaterials: Status, opportunity, and challenge. Prog Mater Sci. 2020;100734. doi: 10.1016/j.pmatsci.2020.100734.
- [68] Manju P, Ajith MR, Jaiswal-Nagar D. Synthesis and characterization of BaZrO₃ nanoparticles by citrate-nitrate sol–gel autocombustion technique: Systematic study for the formation of dense BaZrO₃ ceramics. J Eur Ceram Soc. 2019;39:3756–67. doi: 10.1016/j.jeurceramsoc.2019.03.048.
- [69] Hassan R, Omar S, Balani K. Solid solutioning in ZrB₂ with HfB₂: Effect on densification and oxidation resistance. Int J Refract Met Hard Mater. 2019;84:105041. doi: 10.1016/j.ijrmhm.2019.105041.
- [70] Rajagopalan K, Revathi K, Revathi B, Vishalee S, Manojkumar K, Mujasam Batoo K, et al. Microwave assisted synthesis and characterization of Al_2O_3 . Mater Today Proc. 2022;48(2):160–3. doi: 10. 1016/j.matpr.2020.05.404.
- [71] Choi WJ, Kim JH, Lee H, Park CW, Lee YI, Byun J. Hydrogen reduction behavior of W/Y_2O_3 powder synthesized by ultrasonic spray pyrolysis. Int J Refract Met Hard Mater. 2021;95:105450. doi: 10.1016/j.ijrmhm.2020.105450.
- [72] Rao RR, Dange E, Udayakumar A. Synthesis and slurry spray coating of barium strontium alumino silicate on SiC substrate. Ceram Int. 2021;47(10):14913–22. doi: 10.1016/j.ceramint.2020. 06.311.
- [73] Popov O, Vleugels J, Zeynalov E, Vishnyakov V. Reactive hot pressing route for dense ZrB₂-SiC and ZrB₂-SiC-CNT ultra-high temperature ceramics. J Eur Ceram Soc. 2020;40:5012–9. doi: 10.1016/j.jeurceramsoc.2020.07.039.
- [74] Lozanov VV, Utkin AV, Vasin AA, Sheindlin MA, Baklanova NI. Hot press assisted synthesis and thermophysical properties of iridium intermetallic compounds. Thermochim Acta. 2020;689:178641. doi: 10.1016/j.tca.2020.178641.
- [75] Shaik MA, Golla BR. Mechanical, tribological and electrical properties of ZrB₂ reinforced Cu processed via milling and high-pressure hot pressing. Ceram Int. 2020;46:20226–35. doi: 10. 1016/j.ceramint.2020.05.104.
- [76] Mondi RK, Golla BR. Processing and characterization of super strong and wear resistant Al–5Cu-(0-20 vol%)ZrB₂ composites. J Alloys Compd. 2020;814:152323. doi: 10.1016/j.jallcom.2019. 152323.
- [77] Cotton J. Ultra-high-temperature ceramics. Advanced Materials & Processes. Vol. 168(6), Ohio, United States: ASM International; 2010.
- [78] Pressureless sintering, (n.d), https://www.open.edu/openlearn/ science-maths-technology/engineering-technology/manupedia/ pressureless-sintering accessed February 4, 2021.tle n.d.
- [79] Ghadami S, Taheri-Nassaj E, Baharvandi HR, Ghadami F. Effect of in situ VSi₂ and SiC phases on the sintering behavior and the mechanical properties of HfB₂-based composites. Sci Rep. 2020;10:16540. doi: 10.1038/s41598-020-73295-7.
- [80] Ghazali MSM, Shaifudin MS, Abdullah WRW, Kamaruzzaman WMIWM, Fekeri MFM, Zulkifli MA. Conventional sintering effects on the microstructure and electrical characteristics of low-voltage ceramic varistor. Sintering Technology -Method and Application. London, United Kingdom: IntechOpen Limited; 2018. doi: 10.5772/intechopen.78652.

- [81] Luo C, Zhang Y, Deng T. Pressureless sintering of high performance silicon nitride ceramics at 1,620°C. Ceram Int. 2021;47:29371–8. doi: 10.1016/j.ceramint.2021.07.104.
- [82] Allemand A, Guerin C, Besnard C, Billard R, Le, Petitcorps Y. A comparison between a new ultra fast pressureless sintering (UFPS) technology and spark plasma sintering (SPS) for barium aluminosilicate metastable phase. J Eur Ceram Soc. 2021;41:1524–9. doi: 10.1016/j.jeurceramsoc.2020.09.054.
- [83] Li X, Zhang L, Dong Y, Qin M, Wei Z, Que Z, et al. Towards pressureless sintering of nanocrystalline tungsten. Acta Mater. 2021;220:117344. doi: 10.1016/j.actamat.2021.117344.
- [84] Dehghani H, Khodaei M, Yaghobizadeh O, Ehsani N, Baharvandi HR, Alhosseini SHN, et al. The effect of AlN-Y₂O₃ compound on properties of pressureless sintered SiC ceramics-A review. Int J Refract Met Hard Mater. 2021;95:105420. doi: 10.1016/ j.ijrmhm.2020.105420.
- [85] Nguyen VH, Delbari SA, Ahmadi Z, Shahedi Asl M, Ghassemi Kakroudi M, Le, Van Q, et al. Electron microscopy characterization of porous ZrB2–SiC–AlN composites prepared by pressureless sintering. Ceram Int. 2020;46:25415–23. doi: 10.1016/j.ceramint. 2020.07.011.
- [86] Li X, Zhang L, Dong Y, Gao R, Qin M, Qu X, et al. Pressureless twostep sintering of ultrafine-grained tungsten. Acta Mater. 2020;186:116–23. doi: 10.1016/j.actamat.2020.01.001.
- [87] Jafari S, Bavand-Vandchali M, Mashhadi M, Nemati A. Effects of HfB2 addition on pressureless sintering behavior and microstructure of ZrB₂-SiC composites. Int J Refract Met Hard Mater. 2021;94:105371. doi: 10.1016/j.ijrmhm.2020.105371.
- [88] Tong Z, Ji H, Li X, Liu Z. Microstructure control and optimization of low temperature pressureless sintered silicon nitride-barium aluminosilicate composites. J Eur Ceram Soc. 2020;40:4177–83. doi: 10.1016/j.jeurceramsoc.2020.05.009.
- [89] Qiu S, Li M, Shao G, Wang H, Zhu J, Liu W, et al. (Ca,Sr,Ba)ZrO₃: A promising entropy-stabilized ceramic for titanium alloys smelting. J Mater Sci Technol. 2021;65:82–8. doi: 10.1016/j.jmst. 2020.05.033.
- [90] Ma HB, Xue JX, Zhai JH, Liu T, Ren QS, Liao YH, et al. Pressureless joining of silicon carbide using Ti₃SiC₂ MAX phase at 1,500°C. Ceram Int. 2020;46:14269–72. doi: 10.1016/j.ceramint. 2020.02.155.
- [91] Wu J, Ding C, Xu X, Mi K. Effects of Gd_2O_3 and Yb_2O_3 on the microstructure and performances of O'-Sialon/Si $_3N_4$ ceramics for concentrated solar power. Ceram Int. 2021;47:5054–60. doi: 10.1016/j.ceramint.2020.10.083.
- [92] Wu J, Ding C, Xu X, Chen L. Preparation and thermal stability investigation of Al₂O₃-mullite-ZrO₂-SiC composite ceramics for solar thermal transmission pipelines. Ceram Int. 2021;47(8):10672-8. doi: 10.1016/j.ceramint.2020.12.181.
- [93] Nieai AA, Mohammadi M, Shojaie-Bahaabad M. Hot corrosion behavior of calcium magnesium aluminosilicate (CMAS) on the Yb₂SiO₅-8YSZ composite as a candidate for environmental barrier coatings. Mater Chem Phys. 2020;243:122596. doi: 10.1016/j. matchemphys.2019.122596.
- [94] Xu L, Wang E, Hou X, Chen J, He Z, Liang T. Effect of incorporation of nitrogen on calcium hexaaluminate. J Eur Ceram Soc. 2020;40:6155–61. doi: 10.1016/j.jeurceramsoc.2020.06.057.
- [95] Telle R. The quasi ternary system TiB₂-CrB₂-WB₂ between 1,900 and 2,300°C. J Eur Ceram Soc. 2020;40:341–8. doi: 10.1016/j. jeurceramsoc.2019.09.025.

- [96] Khoeini M, Nemati A, Zakeri M, Shahedi Asl M. Pressureless sintering of ZrB₂ ceramics codoped with TiC and graphite. Int J Refract Met Hard Mater. 2019;81:189–95. doi: 10.1016/j.ijrmhm. 2019.02.026.
- [97] Bahaaddini M, Baharvandi HR, Ehsani N, Khajehzadeh M, Tamadon A. Pressureless sintering of LPS-SiC (SiC-Al₂O₃-Y₂O₃) composite in presence of the B₄C additive. Ceram Int. 2019;45:13536–45. doi: 10.1016/j.ceramint.2019.04.060.
- [98] Ortiz AL, Candelario VM, Moreno R, Guiberteau F. Near-net shape manufacture of B₄C–Co and ZrC–Co composites by slip casting and pressureless sintering. J Eur Ceram Soc. 2017;37:4577–84. doi: 10.1016/j.jeurceramsoc.2017.07.024.
- [99] Sciti D, Brach M, Bellosi A. Long-term oxidation behavior and mechanical strength degradation of a pressurelessly sintered ZrB₂-MoSi₂ ceramic. Scr Mater. 2005;53:1297–302. doi: 10.1016/j. scriptamat.2005.07.026.
- [100] Çalişkan F, Tatli Z, Genson A, Hampshire S. Pressureless sintering of β-SiAlON ceramic compositions using fluorine and oxide additive system. J Eur Ceram Soc. 2012;32:1337–42. doi: 10.1016/j. jeurceramsoc.2011.05.016.
- [101] Telle R. Analysis of pressureless sintering of titanium diboride ceramics with nickel, cobalt, and tungsten carbide additives. J Eur Ceram Soc. 2019;39:2266–76. doi: 10.1016/j.jeurceramsoc.2019. 02.036.
- [102] Ding H, Zhao Z, Qi T, Li X, Ji H. High α - β phase transition and properties of YbF3-added porous Si3N4 ceramics obtained by low temperature pressureless sintering. Int J Refract Met Hard Mater. 2019;78:131–7. doi: 10.1016/j.ijrmhm.2018.09.004.
- [103] Yin J, Huang Z, Liu X, Yan Y, Zhang H, Jiang D. Mechanical properties and in-situ toughening mechanism of pressurelessly densified ZrB₂-TiB₂ ceramic composites. Mater Sci Eng A. 2013;565:414–9. doi: 10.1016/j.msea.2012.12.012.
- [104] Yin J, Zhang H, Yan Y, Huang Z, Liu X, Jiang D. High toughness in pressureless densified ZrB_2 -based composites co-doped with boron-titanium carbides. Scr Mater. 2012;66:523–6. doi: 10.1016/j. scriptamat.2011.12.036.
- [105] Ghaffari SA, Faghihi-Sani MA, Golestani-Fard F, Ebrahimi S. Pressureless sintering of Ta_{0.8}Hf_{0.2}C UHTC in the presence of MoSi₂. Ceram Int. 2013;39:1985–9. doi: 10.1016/j.ceramint.2012. 08.050.
- [106] Liang H, Yao X, Zhang J, Liu X, Huang Z. The effect of rare earth oxides on the pressureless liquid phase sintering of α-SiC. J Eur Ceram Soc. 2014;34:2865–74. doi: 10.1016/j.jeurceramsoc.2014. 03.029.
- [107] Liu C, Sun J, Xie Z. Microstructures and sintering kinetics of pressureless sintered alumina doped with diopside and AlTiB. J Alloys Compd. 2013;546:102–6. doi: 10.1016/j.jallcom.2012.08.097.
- [108] Boccaccini AR, Pearce DH, Trusty PA. Pressureless sintering and characterization of Al₂O₃-platelet-reinforced barium-magnesium aluminosilicate glass-ceramic composites. Compos Part A Appl Sci Manuf. 1997;28:505. doi: 10. 10.1016/S1359-835X(96)00146-7.
- [109] Saeedi Heydari M, Baharvandi HR, Dolatkhah K. Effect of TiO₂ nanoparticles on the pressureless sintering of B₄C-TiB₂ nanocomposites. Int J Refract Met Hard Mater. 2015;51:6–13. doi: 10.1016/j.ijrmhm.2015.01.014.
- [110] Yao M, Chen L, Liu Z, Huo S, Wang S, Wang Y, et al. Two-step sintering of TiB_2 –40wt% TiN composites. Int J Refract Met Hard Mater. 2019;84:105037. doi: 10.1016/j.ijrmhm.2019.105037.
- [111] Arnold JM, Cramer CL, Elliott AM, Nandwana P, Babu SS.
 Microstructure evolution during near-net-shape fabrication of

- Ni_xAl_y-TiC cermets through binder jet additive manufacturing and pressureless melt infiltration. Int J Refract Met Hard Mater. 2019;84:104985. doi: 10.1016/j.ijrmhm.2019.104985.
- [112] Villas-Boas LA, Goulart CA, Kiminami, de Souza RHGA, DPF. A case study of ceramic processing: Microstructural development and electrical properties of Ce_{0.8}Gd_{0.2}O_{1.9}. Ceram Int. 2020;46:12318–28. doi: 10.1016/j.ceramint.2020.01.281.
- [113] Loiu Y-C. Reaction-Sintering Process for Preparing Electronic Ceramics. Recent Patents. Mater Sci. 2015;8:225–38. doi: 10.2174/ 1874464808666150626172915.
- [114] Tsuno K, Irikado H, Hamada K, Kazuhiko O, Ishida J, Suyama S et al. Reaction-sintered silicon carbide: Newly developed material for lightweight mirrors. In: Costeraste J, Armandillo E, editors. European Space Agency. Special Publ. ESA SP, SPIE; 2004. 681–5. doi: 10.1117/12.2307962.
- [115] Gao XJ, Hasigaowa H, Sun MY, Liao CD, Huang WP, Man P, et al. Dynamic compression performance of reaction sintering SiC/B₄C composite. Mater Sci Forum. 2020;999 MSF:83–90. doi: 10.4028/ www.scientific.net/MSF.999.83.
- [116] Luo T, Yang Q, Yu H, Liu J. Formation mechanism and microstructure evolution of Ba₂Ti₉O₂0 ceramics by reaction sintering method. J Am Ceram Soc. 2020;103:1079–87. doi: 10.1111/jace. 16777.
- [117] Goulart CA, Boas LAV, Morelli MR, Souza DPFde. Reactive sintering of yttrium-doped barium zirconate (BaZr_{0.8}Y_{0.2}O₃₋₈) without sintering aids. Ceram Int. 2021;47:2565–71. doi: 10.1016/j. ceramint.2020.09.102.
- [118] Huo S, Wang Y, Yao M, Chen L, Kong Q, Ouyang J, et al. Reactive sintering behavior and enhanced densification of (Ti,Zr)B₂–(Zr,Ti) C composites. J Eur Ceram Soc. 2020;40:4373–80. doi: 10.1016/j. jeurceramsoc.2020.05.037.
- [119] Li L, Wang Q, Liao G, Li K, Ye G. Densification behavior of mullite-Al₂TiO₅ composites by reaction sintering of natural andalusite and TiO₂. Ceram Int. 2018;44:3981–6. doi: 10.1016/j.ceramint.2017. 11.191.
- [120] Moradkhani A, Baharvandi H. Analyzing the microstructures of W-ZrC composites fabricated through reaction sintering and determining their fracture toughness values by using the SENB and VIF methods. Eng Fract Mech. 2018;189:501–13. doi: 10.1016/j. engfracmech.2017.11.038.
- [121] Rodríguez JL, Rodríguez MA, De Aza S, Pena P. Reaction sintering of zircon-dolomite mixtures. J Eur Ceram Soc. 2001;21:343–54. doi: 10.1016/S0955-2219(00)00212-0.
- [122] Suárez M, Fernández A, Menéndez JL, Torrecillas R, Kessel HU, Hennicke J et al. Challenges and opportunities for spark plasma sintering: A key technology for a new generation of materials. Sintering Applications. London, United Kingdom: IntechOpen Limited; 2013. doi: 10.5772/53706.
- [123] Paul TR, Mondal MK, Mallik M. Abrasive Wear Performance and Wear Map of ZrB₂-MoSi₂-SiCw Composites. J Eur Ceram Soc. 2021. doi: 10.1016/j.jeurceramsoc.2021.01.005.
- [124] Saheb N, Iqbal Z, Khalil A, Hakeem AS, Al Aqeeli N, Laoui T, et al. Spark Plasma Sintering of Metals and Metal Matrix Nanocomposites: A Review. J Nanomater. 2012;2012:1–13. doi: 10.1155/2012/983470.
- [125] Chakravarty D, Laxman N, Jayasree R, Mane RB, Mathiazhagan S, Srinivas PVV, et al. Ultrahigh transverse rupture strength in tungsten-based nanocomposites with minimal lattice misfit and dual microstructure. Int J Refract Met Hard Mater. 2021;95:105454. doi: 10.1016/j.ijrmhm.2020.105454.

- [126] Azevêdo HVSB, Raimundo RA, Silva DDS, Morais LMF, Macedo DA, Cavalcante DGL, et al. Microstructure and mechanical properties of Al₂O₃-WC-Co composites obtained by spark plasma sintering. Int J Refract Met Hard Mater. 2021;94:105408. doi: 10.1016/j. ijrmhm.2020.105408.
- [127] Feng L, Fahrenholtz WG, Hilmas GE, Monteverde F. Effect of Nb content on the phase composition, densification, microstructure, and mechanical properties of high-entropy boride ceramics. J Eur Ceram Soc. 2021;41:92–100. doi: 10.1016/j.jeurceramsoc.2020. 08.058.
- [128] Diatta J, Torresani E, Maximenko A, Haines C, Martin D, Olevsky E. Peltier effect during spark plasma sintering of boron carbide. Results Phys. 2021;29:104719. doi: 10.1016/j.rinp.2021.104719.
- [129] Nayebi B, Shahedi Asl M, Akhlaghi M, Ahmadi Z, Tayebifard SA, Salahi E, et al. Spark plasma sintering of TiB₂-based ceramics with Ti₃AlC₂. Ceram Int. 2021;47(9):11929–34. doi: 10.1016/j.ceramint. 2021.01.033.
- [130] Buinevich VS, Nepapushev AA, Moskovskikh DO, Trusov GV, Kuskov KV, Vadchenko SG, et al. Fabrication of ultra-high-temperature nonstoichiometric hafnium carbonitride via combustion synthesis and spark plasma sintering. Ceram Int. 2020;46:16068–73. doi: 10.1016/j.ceramint.2020.03.158.
- [131] Park KB, Park JY, Do Kim Y, Na TW, Mo CB, Choi JI, et al. Spark plasma sintering behavior of TaNbHfZrTi high-entropy alloy powder synthesized by hydrogenation-dehydrogenation reaction. Intermetallics. 2021;130:107077. doi: 10.1016/j.intermet.2020. 107077.
- [132] Jiang Y, Chen J, Liu L, Xu Y, Du J, Tao W, et al. Sintering behavior, infrared spectra and microwave dielectric characteristics analysis for Ce₂Zr₃(MoO₄)₉ ceramics achieved by reaction-sintering method. J Alloys Compd. 2021;875:160096. doi: 10.1016/j.jallcom. 2021 160096
- [133] Sun SK, Stennett MC, Corkhill CL, Hyatt NC. Reactive spark plasma synthesis of $CaZrTi_2O_7$ zirconolite ceramics for plutonium disposition. J Nucl Mater. 2018;500:11–4. doi: 10.1016/j.jnucmat.2017. 12.021.
- [134] Rominiyi AL, Shongwe MB, Jeje SO, Olubambi PA. Microstructure, tribological and oxidation behaviour of spark plasma sintered Ti-Ni-xTiCN composites. J Alloys Compd. 2022;890:161857. doi: 10.1016/j.jallcom.2021.161857.
- [135] https://en.wikipedia.org/wiki/Hot_pressing. accessed May 08, 2023 n.d.
- [136] HIPing What Is It and What are The Advantages for Engineering Ceramics? n.d https://www.azom.com/article.aspx ? ArticleID = 5769 accessed February 5, 2021.
- [137] Viswanathan V, Laha T, Balani K, Agarwal A, Seal S. Challenges and advances in nanocomposite processing techniques. Mater Sci Eng R Reports. 2006;54:121–285. doi: 10.1016/j.mser.2006.11.002.
- [138] Kang N, Lu JL, Li QG, Cao YN, Lin X, Wang LL, et al. A new way to net-shaped synthesis tungsten steel by selective laser melting and hot isostatic pressing. Vacuum. 2020;179:109557. doi: 10.1016/ j.vacuum.2020.109557.
- [139] Sun C, Guo Y, Yang Z, Li J, Xi S, Jie Z, et al. Microstructurally stable nanocomposite WTaMoNb/Cu prepared by mechanical alloying and hot pressing sintering. Mater Lett. 2022;306:130894. doi: 10.1016/j.matlet.2021.130894.
- [140] Moustafa S, Daoush W, Ibrahim A, Neubaur E. Hot forging and hot pressing of AlSi powder compared to conventional powder metallurgy route. Mater Sci Appl. 2011;02:1127–33. doi: 10.4236/ msa.2011.28152.

- [141] Li J, Ren X, Zhang Y, Hou H. Silicon carbide hot pressing sintered by magnesium additive: microstructure and sintering mechanism. J Mater Res Technol. 2020;9:520–9. doi: 10.1016/j. jmrt.2019.10.081.
- [142] Dobrzanski LA, Dobrzanska-Danikiewicz AD, Achtelik-Franczak A, Dobrzanski LB, Hajduczek E, Matula G. Fabrication technologies of the sintered materials including materials for medical and dental application. Powder Metallurgy - Fundamentals and Case Studies. London, United Kingdom: IntechOpen Limited; 2017. doi: 10.5772/65376.
- [143] Šajgalík P, Cheng, Han X, Zhang C, Hanzel O, Sedláček J, et al. Ultra-high creep resistant SiC ceramics prepared by rapid hot pressing. J Eur Ceram Soc. 2022;42:820–9. doi: 10.1016/j. ieurceramsoc.2021.11.010.
- [144] Wakai F, Okuma G, Mücke R, Guillon O. Modelling of elimination of strength-limiting defects by pressure-assisted sintering at low stress levels. J Eur Ceram Soc. 2021;41:202. doi: 10. 10.1016/j. jeurceramsoc.2021.09.040.
- [145] Kaplanskii YY, Levashov EA, Korotitskiy AV, Loginov PA, Sentyurina ZA, Mazalov AB. Influence of aging and HIP treatment on the structure and properties of NiAl-based turbin blades manufactured by laser powder bed fusion. Addit Manuf. 2020;31:100999. doi: 10.1016/j.addma.2019.100999.
- [146] Lv S, Zu Y, Chen G, Fu X, Zhou W. An ultra-high strength CrMoNbWTi-C high entropy alloy co-strengthened by dispersed refractory IM and UHTC phases. J Alloys Compd. 2019;788:1256–64. doi: 10.1016/j.jallcom.2019.02.318.
- [147] Herrmann M, Räthel J. Hot pressing and hot isostatic pressing. Encyclopedia of materials: technical ceramics and glasses. Amsterdam, Netherlands: Elsevier; 2021. p. 270–7. doi: 10.1016/B978-0-12-818542-1.00039-4.
- [148] Dhand V, Yadav, Kim SH, Rhee KY. A comprehensive review on the prospects of multi-functional carbon nano onions as an effective, high-performance energy storage material. Carbon. 2021;175:534–75. doi: 10.1016/j.carbon.2020.12.083.
- [149] Dhand V, Hong SK, Li L, Kim J-M, Kim SH, Rhee KY, et al. Fabrication of robust, ultrathin and light weight, hydrophilic, PVDF-CNT membrane composite for salt rejection. Compos Part B Eng. 2019;160:632–43. doi: 10.1016/j.compositesb.2018.12.106.
- [150] Dhand V, Bharadwaj S, Amareshwari K, Himabindu V, Rhee KY, Park S-J, et al. Facile, soot free approach toward synthesis of carbon nanoropes via chemical vapor deposition of acetylene in the presence of MnFe₂O₄ coated on stainless steel. Appl Surf Sci. 2015;359:797–804. doi: 10.1016/j.apsusc.2015.10.208.
- [151] Dhand V, Venkateswer Rao M, Mittal G, Rhee KY, Park SJ. Synthesis of lithium–graphite nanotubes – An in-situ CVD approach using organo-lithium as a precursor in the presence of copper. Curr Appl Phys. 2015;15:265–73. doi: 10.1016/j.cap.2014. 12.019.
- [152] Dhand V, Mittal G, Rhee KY, Park SJ. Synthesis and comparison of different spinel ferrites and their catalytic activity during chemical vapor deposition of polymorphic nanocarbons. Int J Precis Eng Manuf Technol. 2017;4:441–51. doi: 10.1007/s40684-017-0049-3.
- [153] Patil DS, Kar R, Chopade SS. Cold plasma processing of materials for extreme conditions. Matter under extreme conditions. Amsterdam, Netherlands: Elsevier; 2017. p. 411–69. doi: 10.1016/ B978-0-12-801300-7.00012-7.
- [154] He Q, Li H, Yin X, Lu J. Large-scale synthesis of SiC/PyC core-shell structure nanowires via chemical liquid-vapor deposition. Ceram Int. 2021;47:500–9. doi: 10.1016/j.ceramint.2020.08.157.

- [155] Ren J, Feng E, Zhang Y, Zhang J, Ding D, Li L. Influences of deposition temperature, gas flow rate and ZrC content on the microstructure and anti-ablation performance of CVD-HfC-ZrC coating. Ceram Int. 2021;47:556–66. doi: 10.1016/j.ceramint.2020. 08.163.
- [156] Tanaka K, Liao ME, Aleman A, Zaid H, Goorsky MS, Kodambaka S. Growth of heterolayered [cubic-TaC(111) + rhombohedral-Ta3C2(0001)] nanocomposite thin films on Al_2O_3 (0001). Acta Mater. 2021;204:116499. doi: 10.1016/j.actamat.2020.116499.
- [157] Yu F, Xu J, Li H, Wang Z, Sun L, Deng T, et al. Ga-In liquid metal nanoparticles prepared by physical vapor deposition. Prog Nat Sci Mater Int. 2018;28:28–33. doi: 10.1016/j.pnsc.2017.12.004.
- [158] Avino F, Fonnesu D, Koettig T, Bonura M, Senatore C, Perez Fontenla AT, et al. Improved film density for coatings at grazing angle of incidence in high power impulse magnetron sputtering with positive pulse. Thin Solid Films. 2020;706:138058. doi: 10.1016/j.tsf.2020.138058.
- [159] Kulkarni R, Rondiya S, Pawbake A, Waykar R, Jadhavar A, Jadkar V, et al. Structural and optical properties of CdTe thin films deposited using RF magnetron sputtering. Energy Procedia. 2017;110:188–95. doi: 10.1016/j.egypro.2017.03.126.
- [160] Mundra SS, Pardeshi SS, Bhavikatti SS, Nagras A. Development of an integrated physical vapour deposition and chemical vapour deposition system. Mater Today Proc. 2021;46:1229–34. doi: 10.1016/j.matpr.2021.02.069.
- [161] Herman E, Stewart JA, Dingreville R. A data-driven surrogate model to rapidly predict microstructure morphology during physical vapor deposition. Appl Math Model. 2020;88:589–603. doi: 10.1016/j.apm.2020.06.046.
- [162] Kameneva A, Antonova N, Pesin M, Makarov V, Nikitin S, Bublik N. Structural and phase transformations control in Ti and Al cathode materials, WC–Co substrate, and Ti_{1-x}Al_xN coating to improve their physico-mechanical and wear properties. Int J Refract Met Hard Mater. 2022;102:105726. doi: 10.1016/j.ijrmhm. 2021.105726.
- [163] Jokanović V, Bundaleski N, Petrović B, Ferarra M, Jokanović B, Živković S, et al. Detailed physico-chemical characterization of the multilayered thin films based on titanium oxynitride and copper doped titanium nitride obtained by different PVD techniques. Vacuum. 2022;195:110708. doi: 10.1016/j.vacuum.2021.110708.
- [164] Kumar S, Mondal S, Kumar A, Ranjan A, Prasad NE. Chemical vapor deposition of TaC/SiC on graphite tube and its ablation and microstructure studies. Coatings. 2017;7:101. doi: 10.3390/ coatings7070101.
- [165] Zhu Y, Cheng L, Li M, Ma B, Liu Y, Zhang L. The synthesis and characterization of CVD ZrB₂ coating from ZrCl₄-BCl₃-H₂-Ar system. Ceram Int. 2018;44:2002–10. doi: 10.1016/j.ceramint.2017.10.145.

- [166] Zhu Y, Cheng L, Gao S, Li J, Deng J, Zhang L. Thermodynamic analysis on the codeposition of ZrC-SiC by chemical vapor deposition using the ZrCl₄-C₃H₆-MTS-H₂-Ar system. Ceram Int. 2014;40:6427–33. doi: 10.1016/j.ceramint.2013.11.091.
- [167] Moraes V, Fuger C, Paneta V, Primetzhofer D, Polcik P, Bolvardi H, et al. Substoichiometry and tantalum dependent thermal stability of α-structured W–Ta–B thin films. Scr Mater. 2018;155:5–10. doi: 10.1016/j.scriptamat.2018.06.005.
- [168] Startt J, Kustas A, Pegues J, Yang P, Dingreville R. Compositional effects on the mechanical and thermal properties of MoNbTaTi refractory complex concentrated alloys. Mater Des. 2022;213:110311. doi: 10.1016/j.matdes.2021.110311.
- [169] Alvi S, Jarzabek DM, Kohan MG, Hedman D, Jenczyk P, Natile MM, et al. Synthesis and mechanical characterization of a CuMoTaWV high-entropy film by magnetron sputtering. ACS Appl Mater Interfaces. 2020;12:21070–9. doi: 10.1021/acsami.0c02156.
- [170] Dan A, Chattopadhyay K, Barshilia HC, Basu B. Shifting of the absorption edge in TiB₂/TiB(N)/Si₃N₄ solar selective coating for enhanced photothermal conversion. Sol Energy. 2018;173:192–200. doi: 10.1016/j.solener.2018.07.002.
- [171] Yang X, Zhao-hui C, Feng C. High-temperature protective coatings for C/SiC composites. J Asian Ceram Soc. 2014;2:305–9. doi: 10. 1016/j.jascer.2014.07.004.
- [172] Tkachenko LA, Shaulov AY, Berlin AA. High-temperature protective coatings for carbon fibers. Inorg Mater. 2012;48:213–21. doi: 10.1134/S0020168512030168.
- [173] Fahrenholtz WG, Hilmas GE. Ultra-high temperature ceramics: Materials for extreme environments. Scr Mater. 2017;129:94–9. doi: 10.1016/j.scriptamat.2016.10.018.
- [174] Guria JF, Bansal A, Kumar V. Effect of additives on the thermal conductivity of zirconium diboride based composites – A review. J Eur Ceram Soc. 2021;41:1–23. doi: 10.1016/j.jeurceramsoc.2020. 08.051.
- [175] Arai Y, Inoue R, Goto K, Kogo Y. Carbon fiber reinforced ultra-high temperature ceramic matrix composites: A review. Ceram Int. 2019;45:14481–9. doi: 10.1016/j.ceramint.2019.05.065.
- [176] Ch JR, Vetrivendan E, Madhura B, Ningshen S. A review of ceramic coatings for high temperature uranium melting applications. J Nucl Mater. 2020;540:152354. doi: 10.1016/j.jnucmat.2020.152354.
- [177] Asl MS, Nayebi B, Ahmadi Z, Zamharir MJ, Shokouhimehr M. Effects of carbon additives on the properties of ZrB₂-based composites: A review. Ceram Int. 2018;44:7334–48. doi: 10.1016/j. ceramint.2018.01.214.
- [178] Hu ZY, Zhang ZH, Cheng XW, Wang FC, Zhang YF, Li SL A review of multi-physical fields induced phenomena and effects in spark plasma sintering: Fundamentals and applications. Mater Des. 2020;191:108662. doi: 10.1016/j.matdes.2020.108662.